Debye Lecture 8

Self-Assembled Nanocrystal Superlattices: Preparation and Properties.

C. B. Murray

Designing Nanoscale Materials

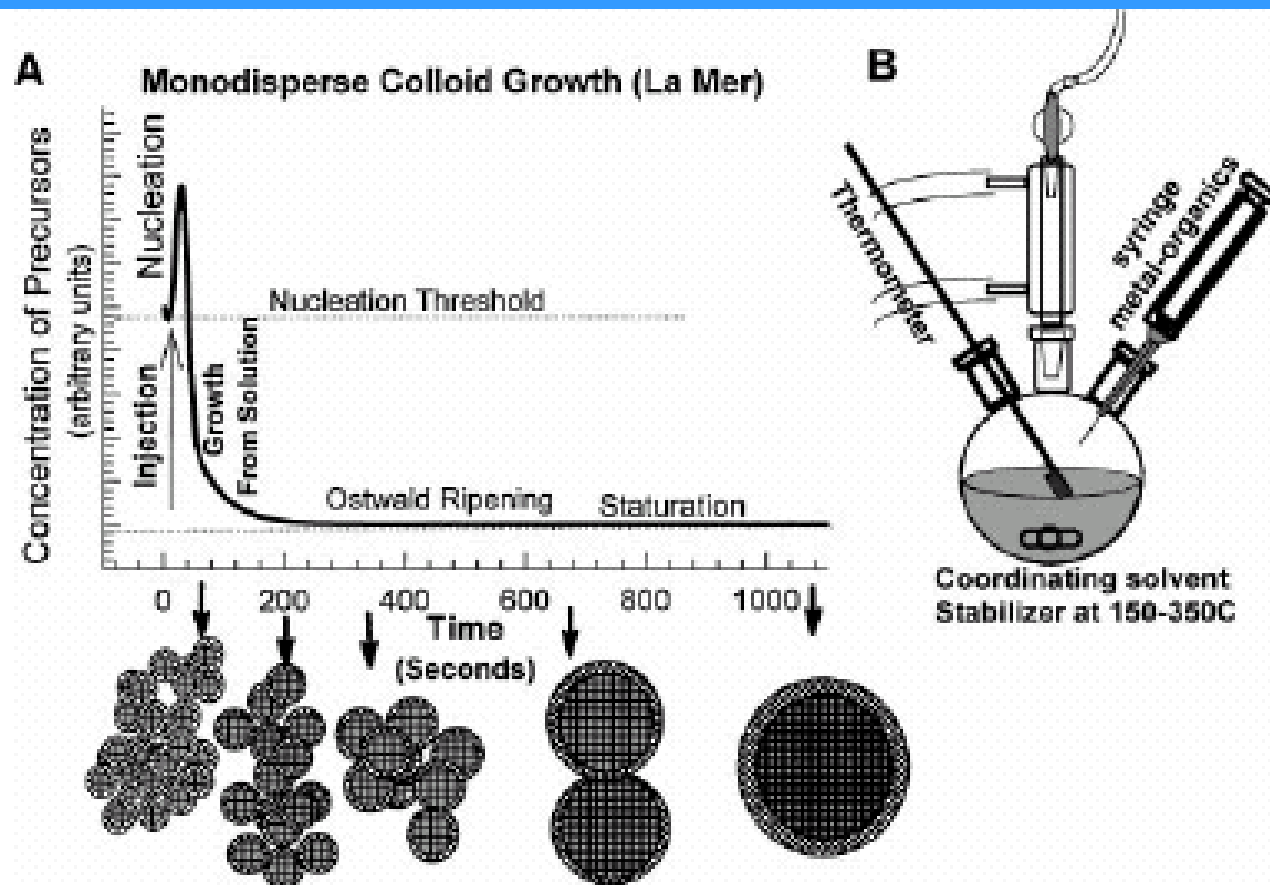## Lecture Series by 2004 Debye Institute Professor

Christopher B. Murray

IBM Research

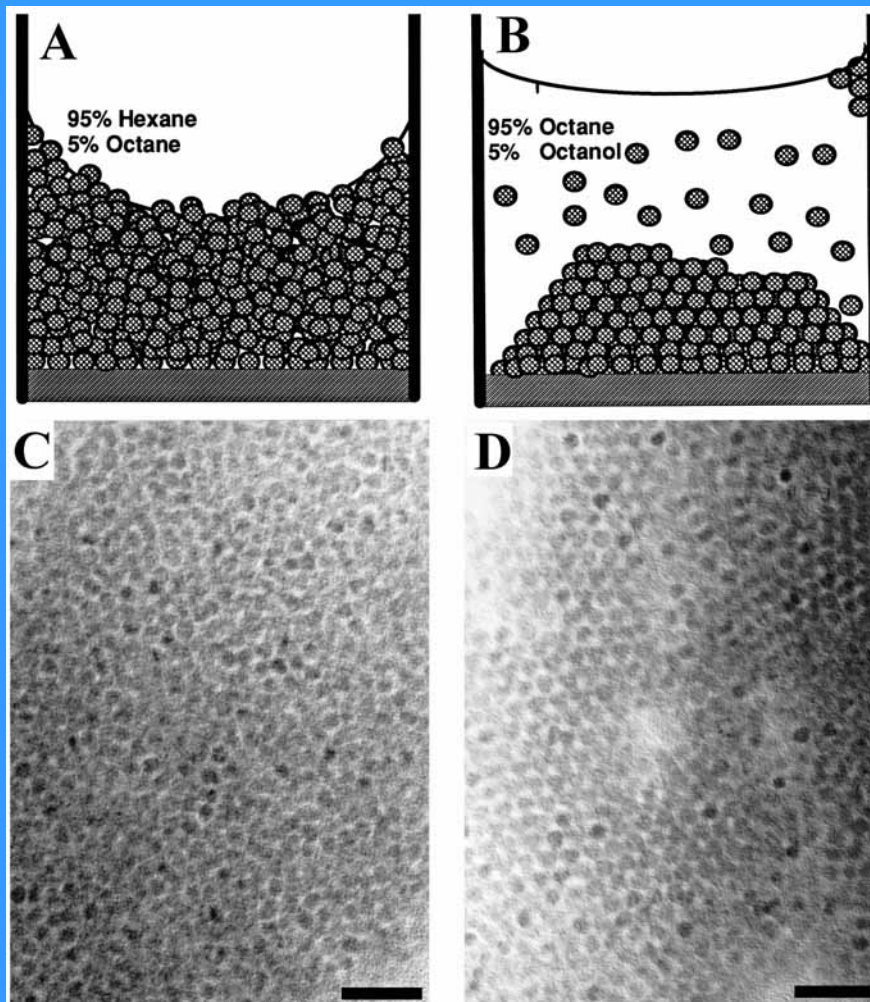Ornstein Laboratory 166

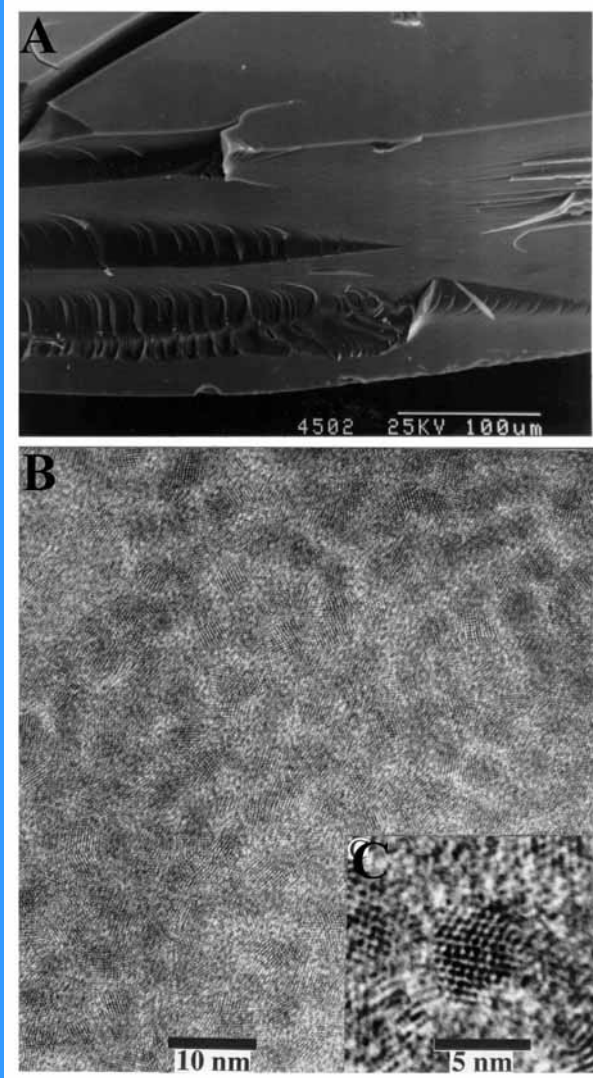Office phone 253 2227

cbmurray@alum.mit.edu

A Monodisperse Colloid Growth (La Mer)

Concentration of Precursors (arbitrary units)

Nucleation

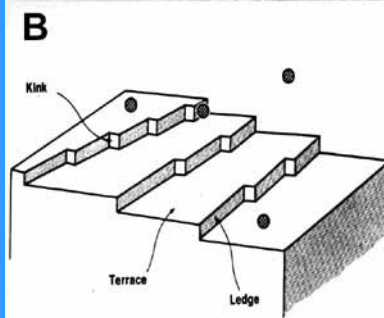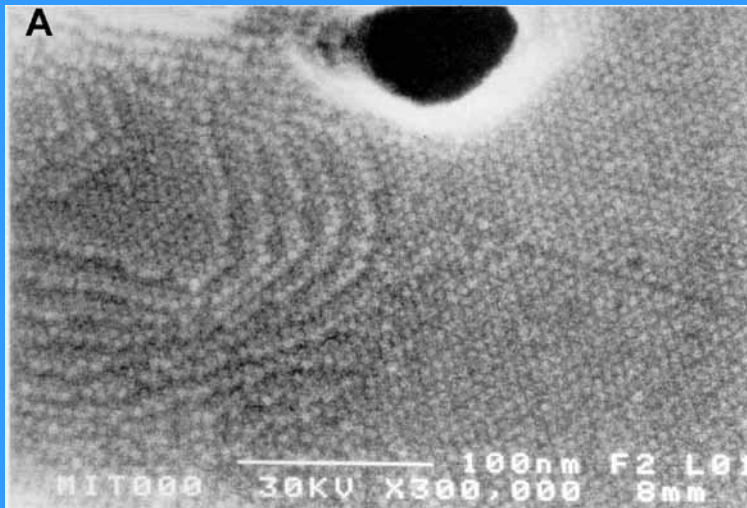Nucleation Threshold

Injection

Growth From Solution

Ostwald Ripening   Staturation

0   200   400   600   800   1000

Time (Seconds)

B

Thermometer

syringe metal-organics
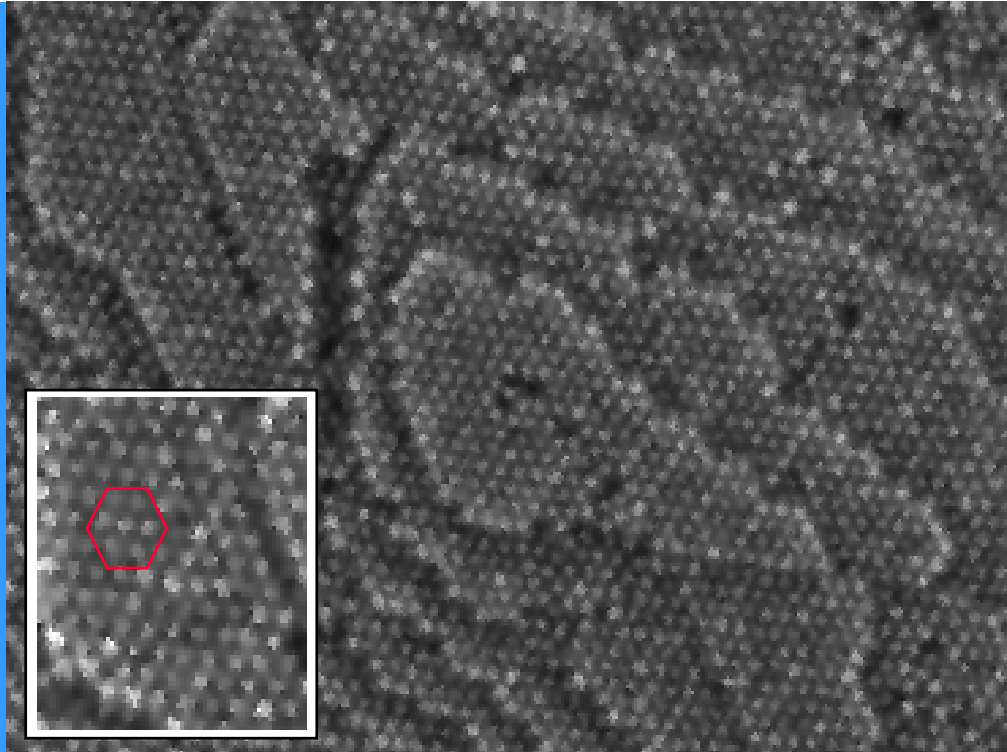
Coordinating solvent Stabilizer at 150-350C

Figure 1 (*A*) Cartoon depicting the stages of nucleation and growth for the preparation of monodisperse NCs in the framework of the La Mer model. As NCs grow with time, a size series of NCs may be isolated by periodically removing aliquots from the reaction vessel. (*B*) Representation of the simple synthetic apparatus employed in the preparation of monodisperse NC samples.
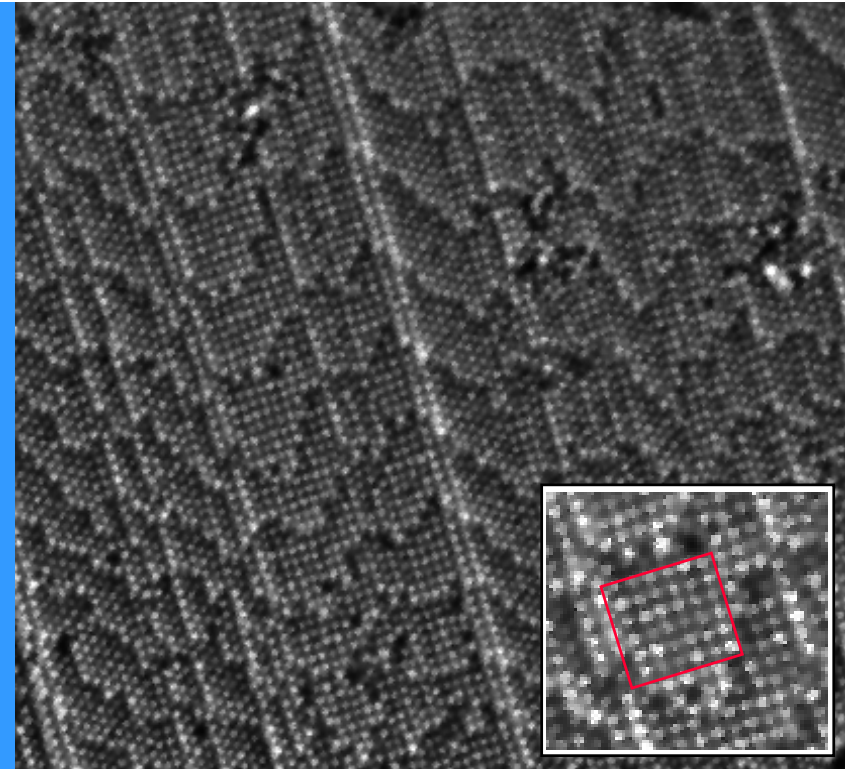
A
95% Hexane
5% Octane

B
95% Octane
5% Octanol

C

D

A

100nm F2 L01
MIT000 30KV X300,000 8mm

B

Kink

Terrace

Ledge

C

200A
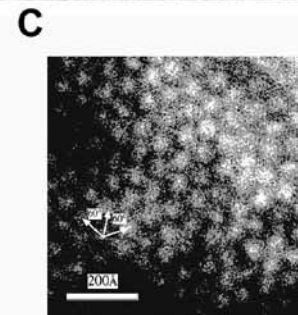
Cobalt Nanocrystal Superlattices (T. Betley et al)
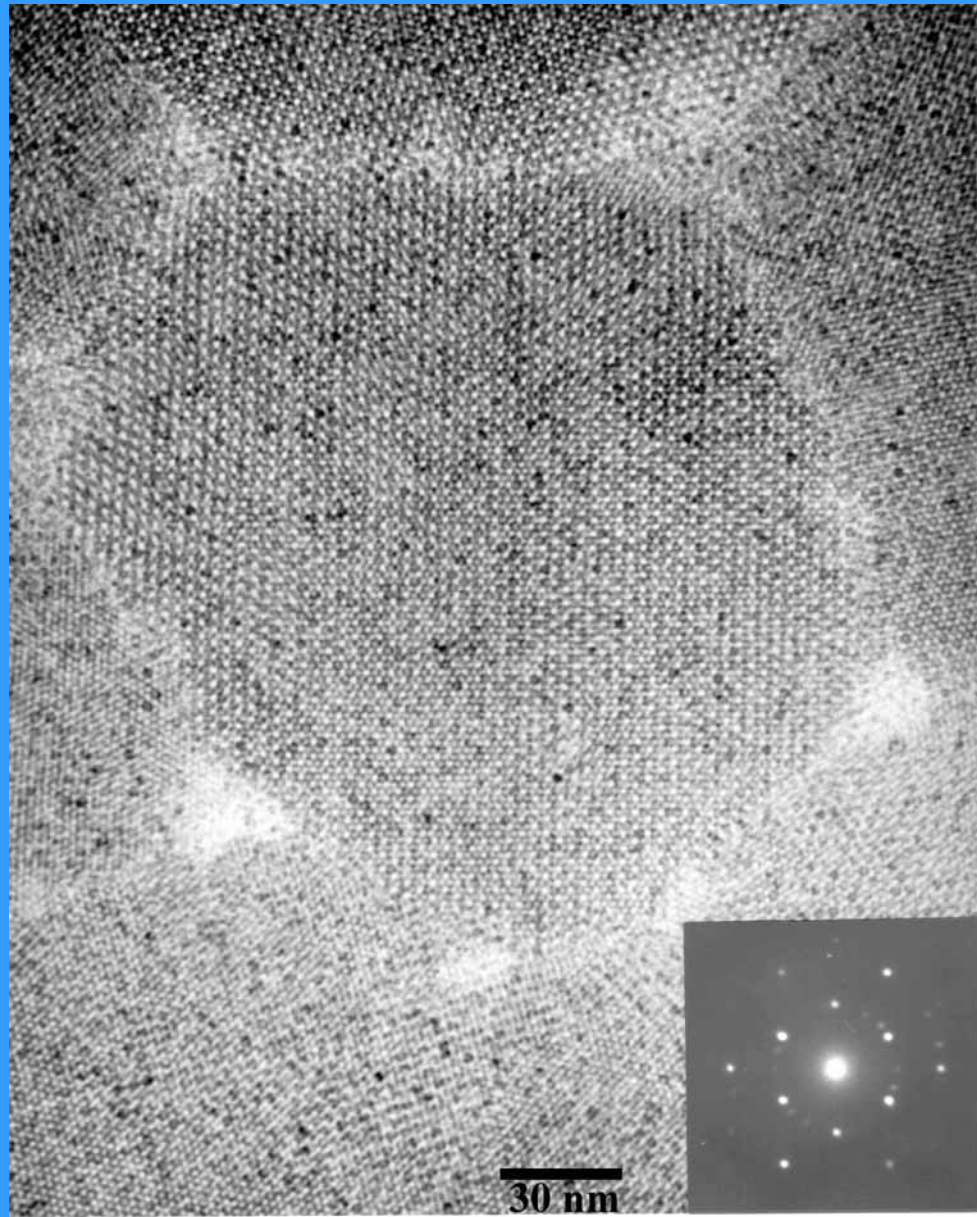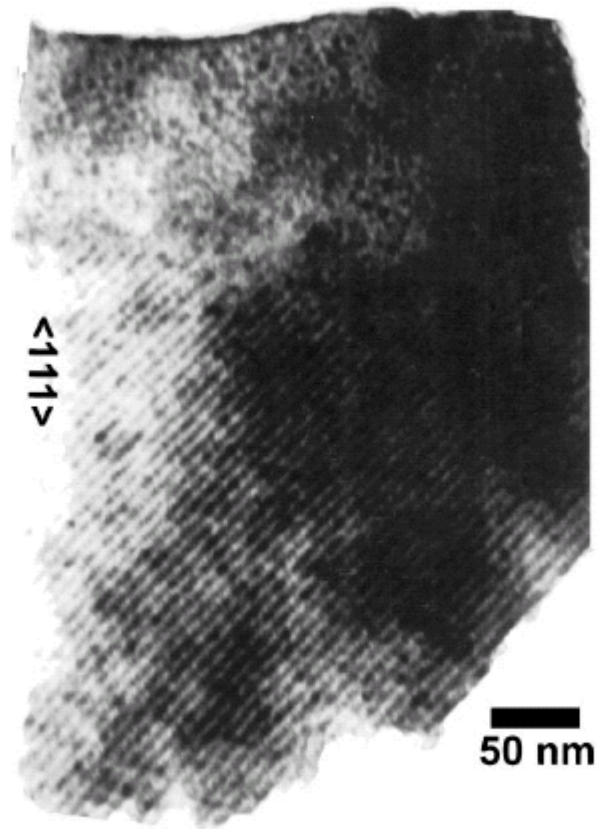
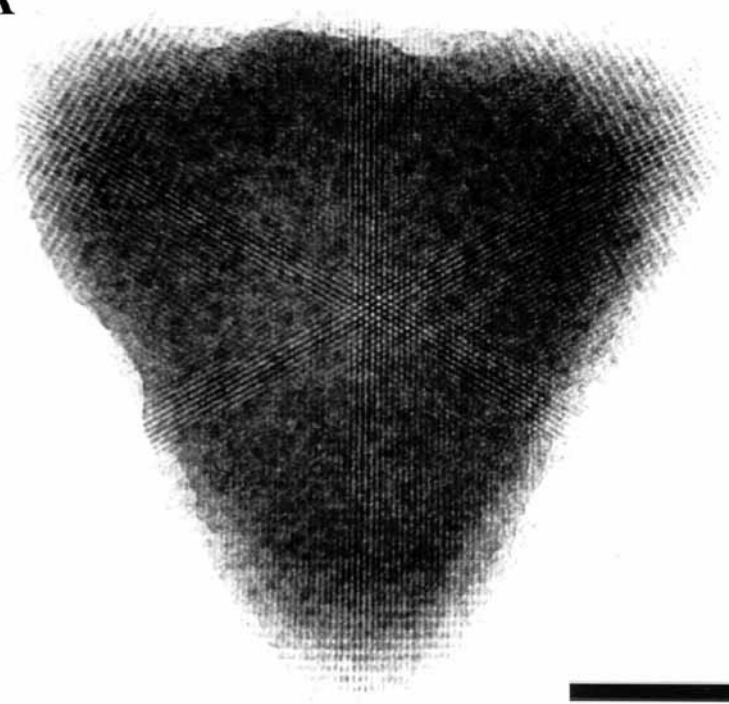

Hexagonal packing

Cubic packing

10 nm Cobalt NCs
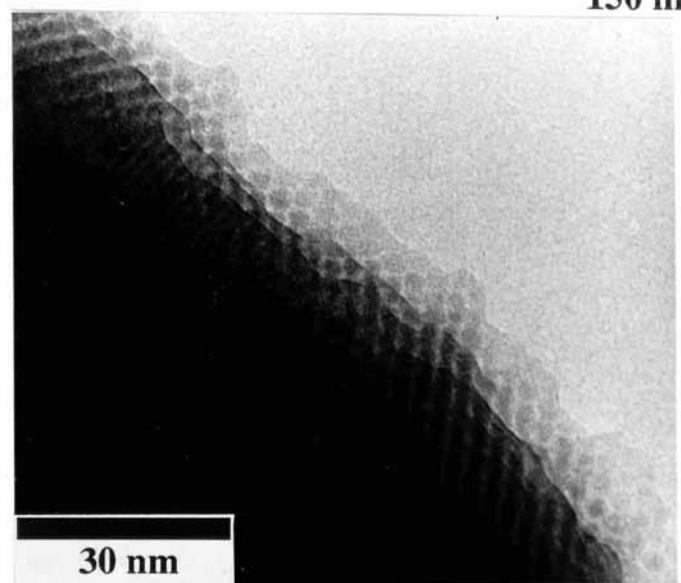
30 nm

50 nm
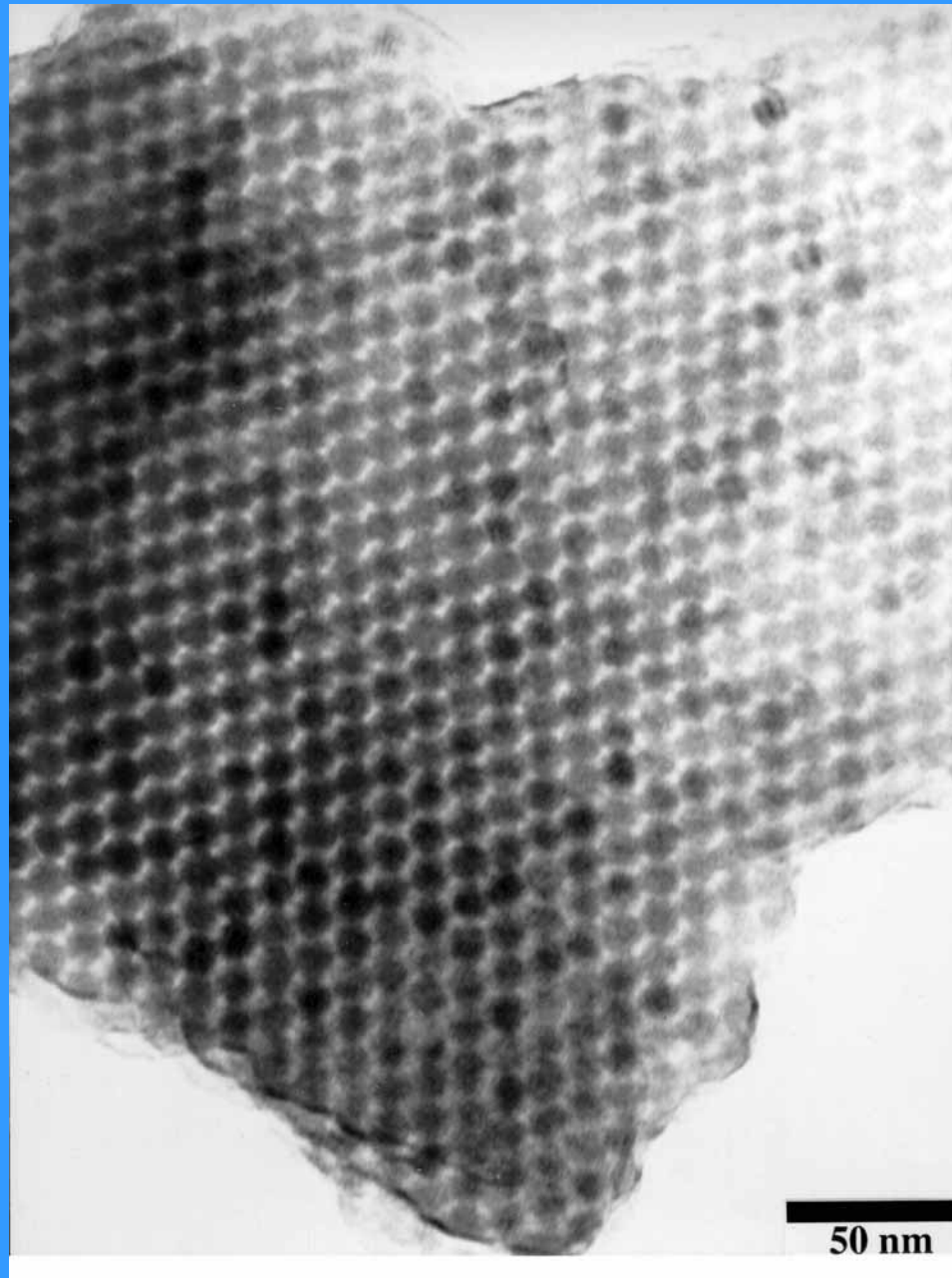
Figure 13 TEM cross-section through a (111)-oriented island of 100 Å CdSe NCs. The sample was cleaved along the (111) axis. The top of the image shows a glassy region formed at high growth rates. The bottom shows the long-range order possible at slower growth rates. Striations seen of the $(112)_{SL}$ fcc planes.
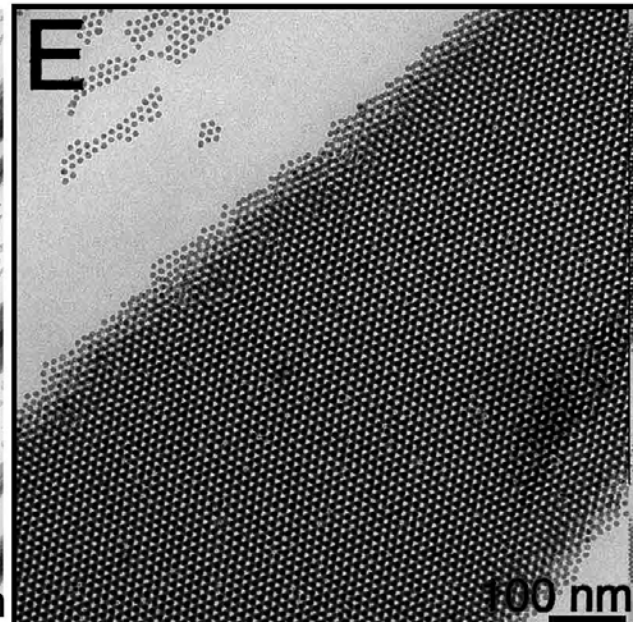
A

B
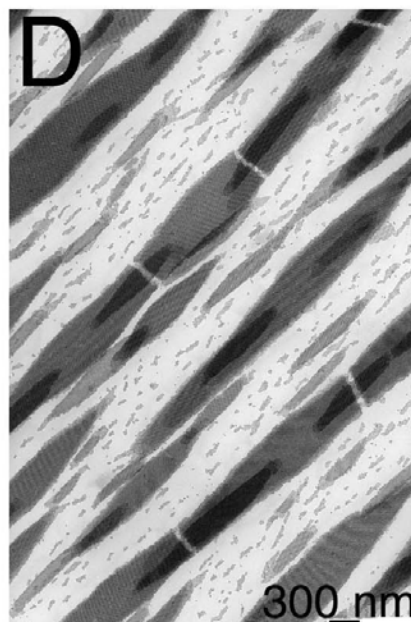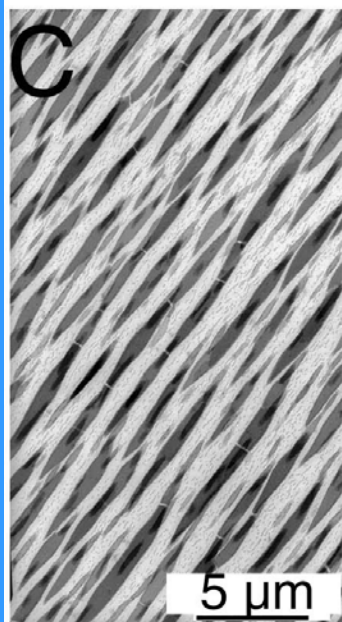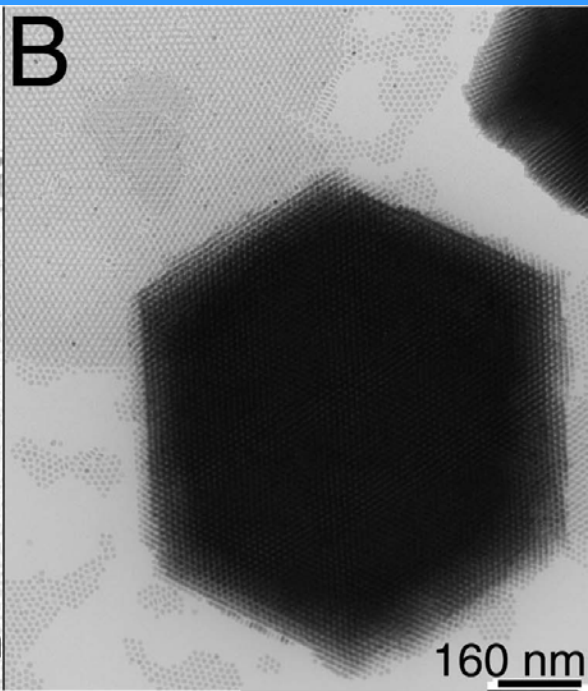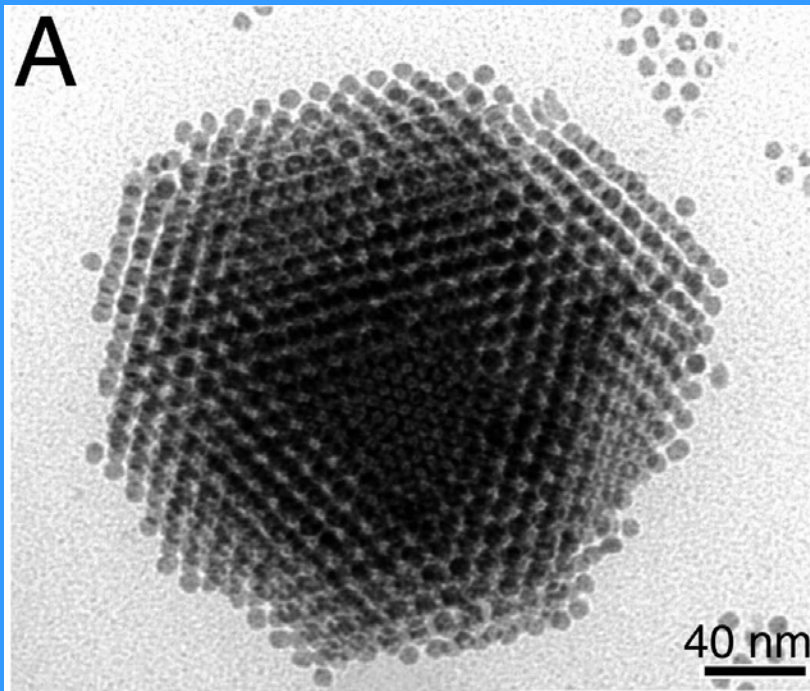
150 nm
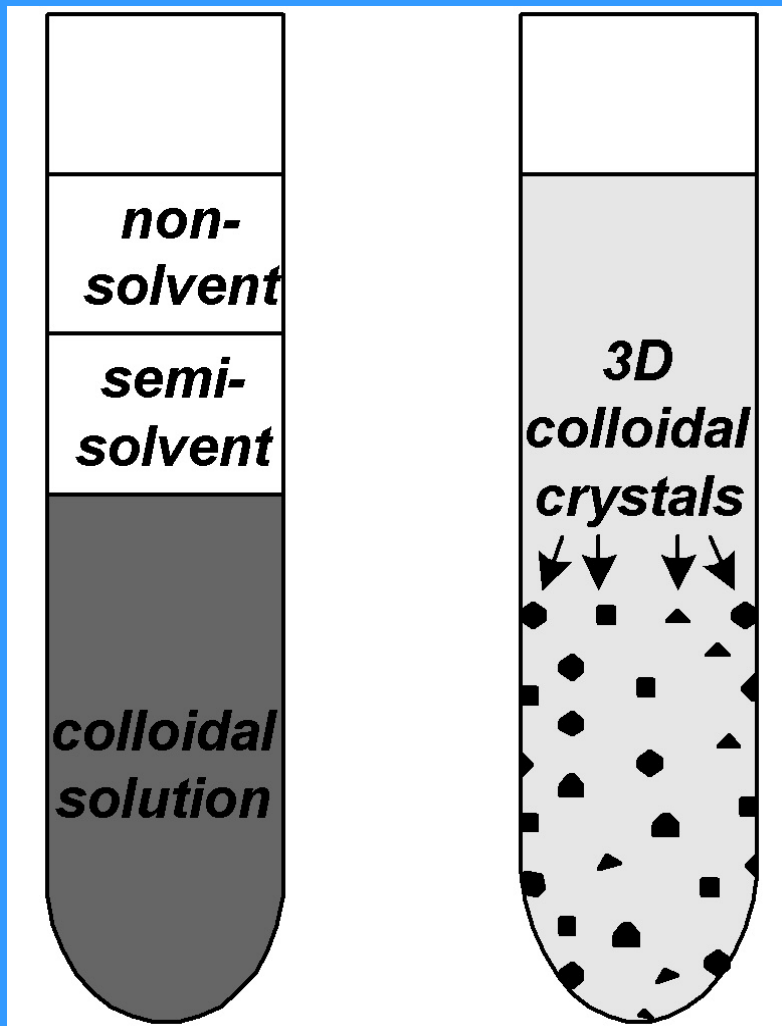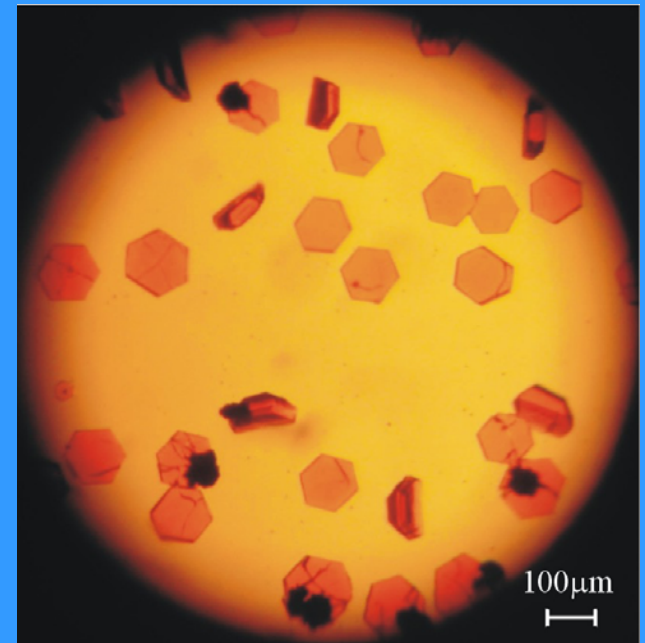
30 nm

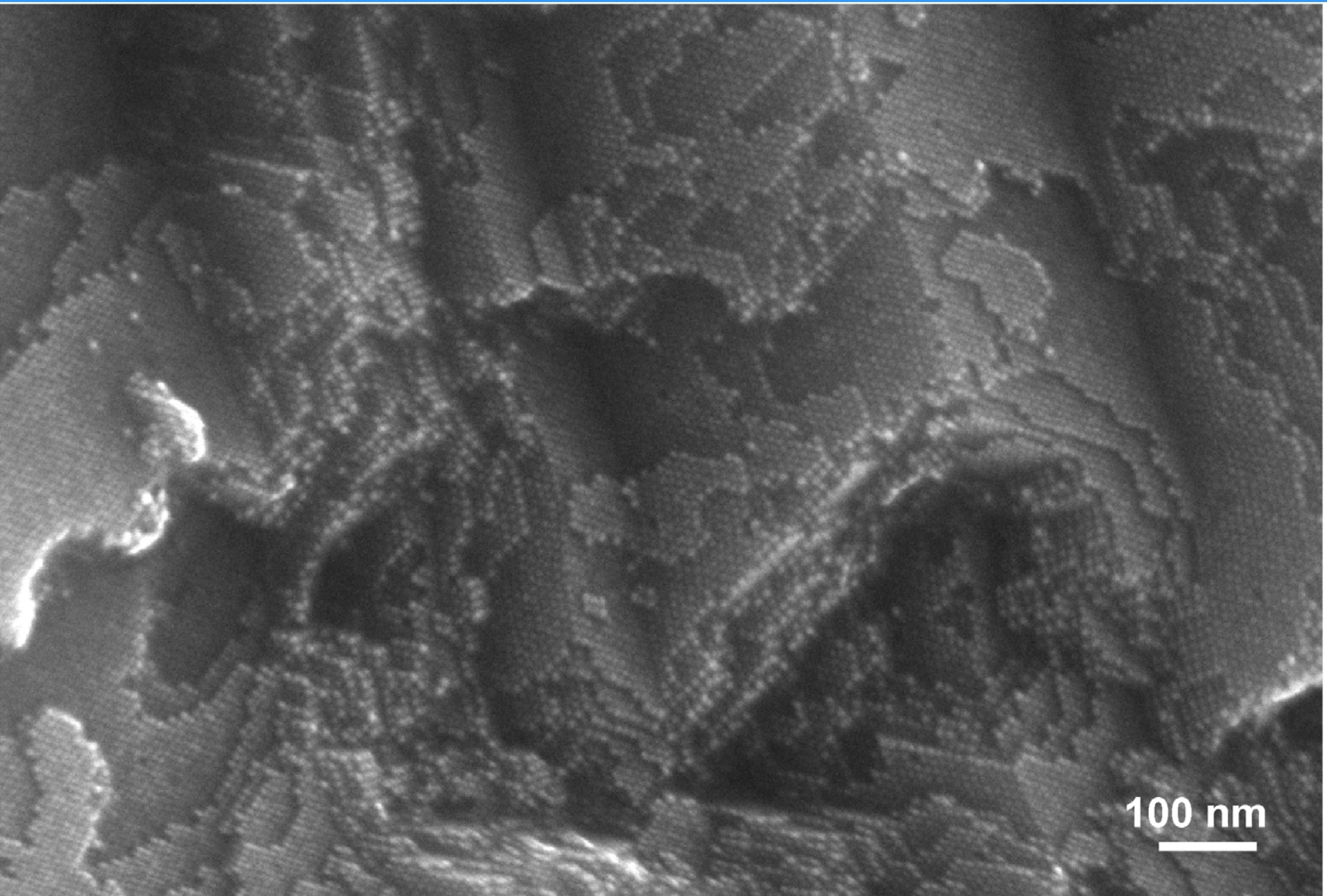# 3D Colloidal supercrystals of nanocrystals

Crystallisation at the liquid - liquid interface leads to formation of perfectly facetted colloidal crystals
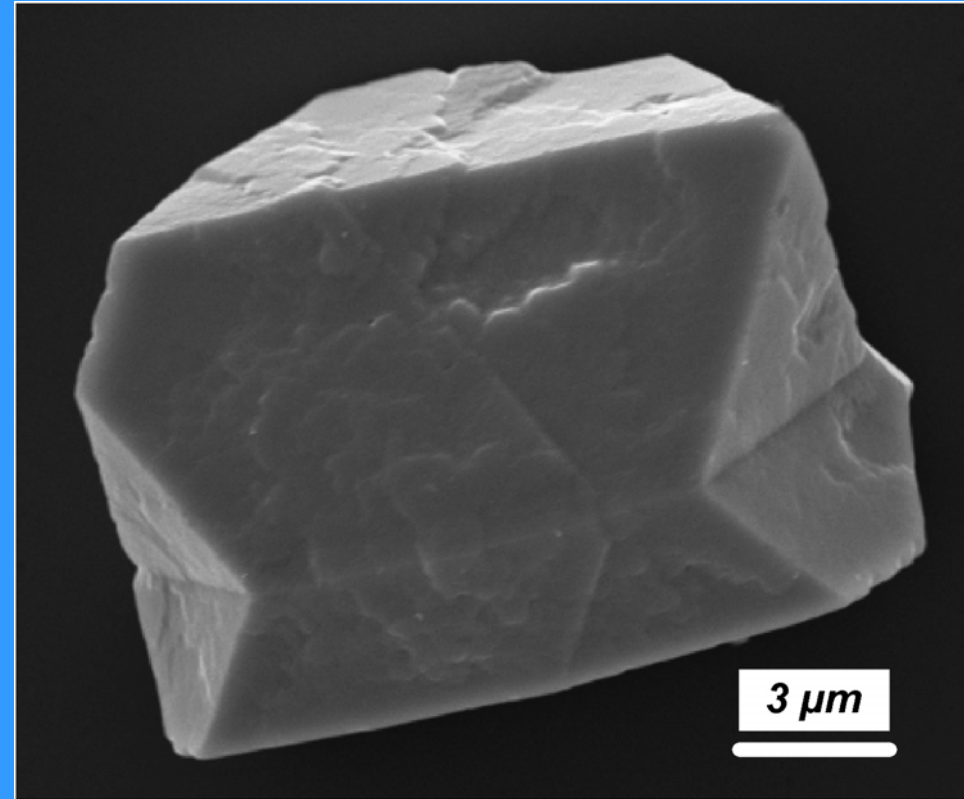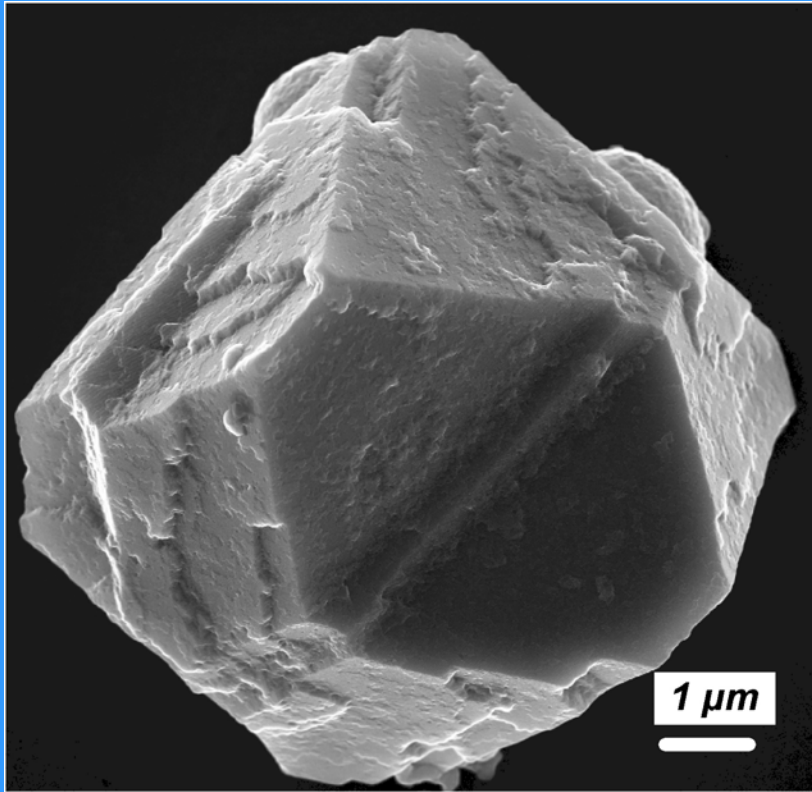
*Optical micrograph of **CdSe** 3D colloidal crystals*

100 nm

Three-dimensional colloidal supercrystals of CoPt$_3$ nanocrystals

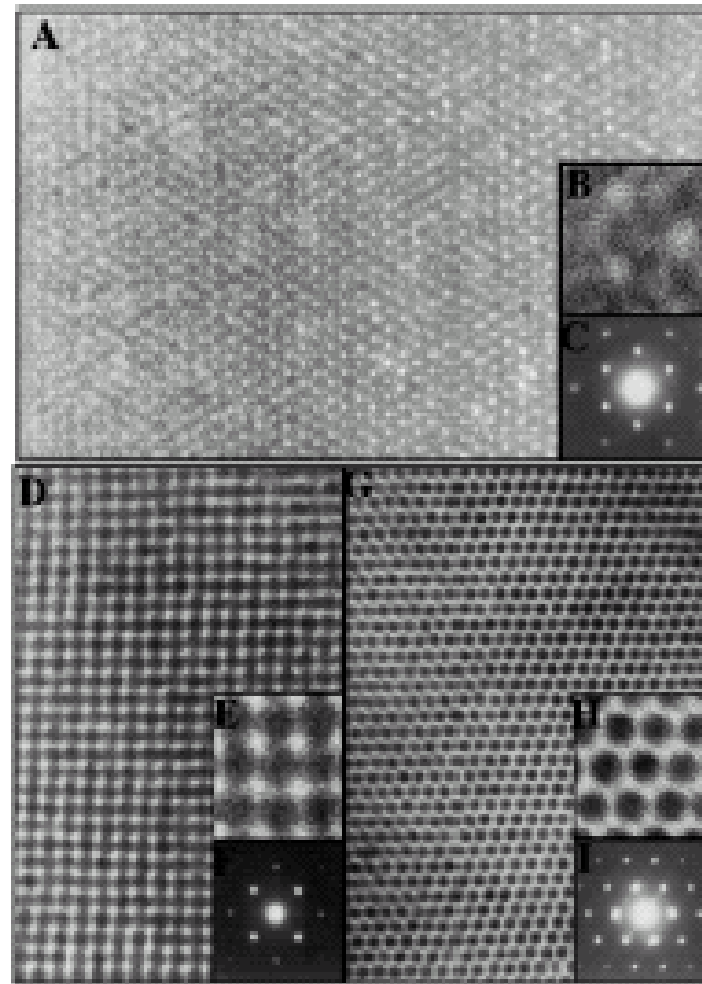*Institute of Physical Chemistry, University of Hamburg, Hamburg, Germany*

Figure 20 (A) TEM image of a (100)_{SL} projection through a three-dimensional super-lattice of 48 Å CdSe NCs. (B) At high magnification, the internal lattice structure of the NC building blocks is resolved. (C) Small-angle electron diffraction pattern demonstrates the lateral perfection of the superlattice domain. (D) TEM image showing the (101)_{SL} projection for a superlattice of 48 Å CdSe NCs. (E) High magnification shows lattice imaging of the individual NCs. (F) Small-angle electron diffraction demonstrates the perfection of another characteristic fcc orientation. (G) TEM image of an fcc superlattice of 64 Å CdSe NCs viewed along the (111)_{SL} axis. Inset (H) higher magnification image showing the individual NCs in the superlattice and (I) a small-angle electron diffraction pattern showing ordering in the (111)_{SL} orientation over the probed 2 μm area.
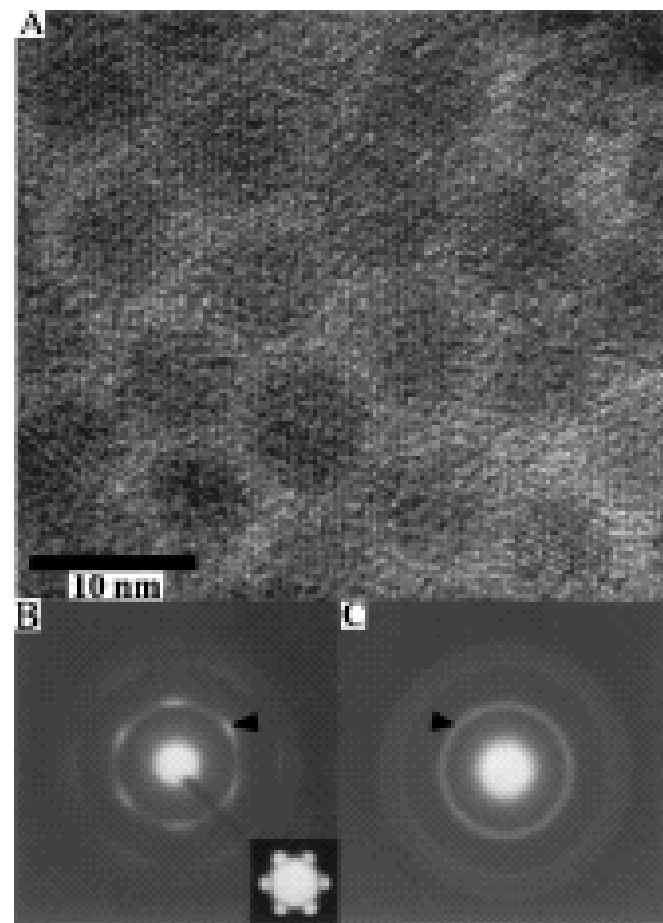
Figure 22 (*A*) High resolution TEM image shows a section of a [111]$_{SL}$-oriented superlattice of 62 Å CdSe NCs. The periodic dot pattern running through the image arises from the coherent imaging of columns of Cd and Se atoms making up the NCs in the superlattice. (*B*) Wide-angle electron diffraction pattern from a ~2 μm area. Strong modulation of the diffraction pattern results from the preferred alignment of the individual NC axes within the superlattice. At lower flux, the small-angle electron diffraction pattern can be seen emerging from the central beam. (*C*) Wide-angle electron diffraction pattern from a NC glass, having an isotropic orientation of NCs, is prepared from the same NC sample.

100 nm

50nm

500nm
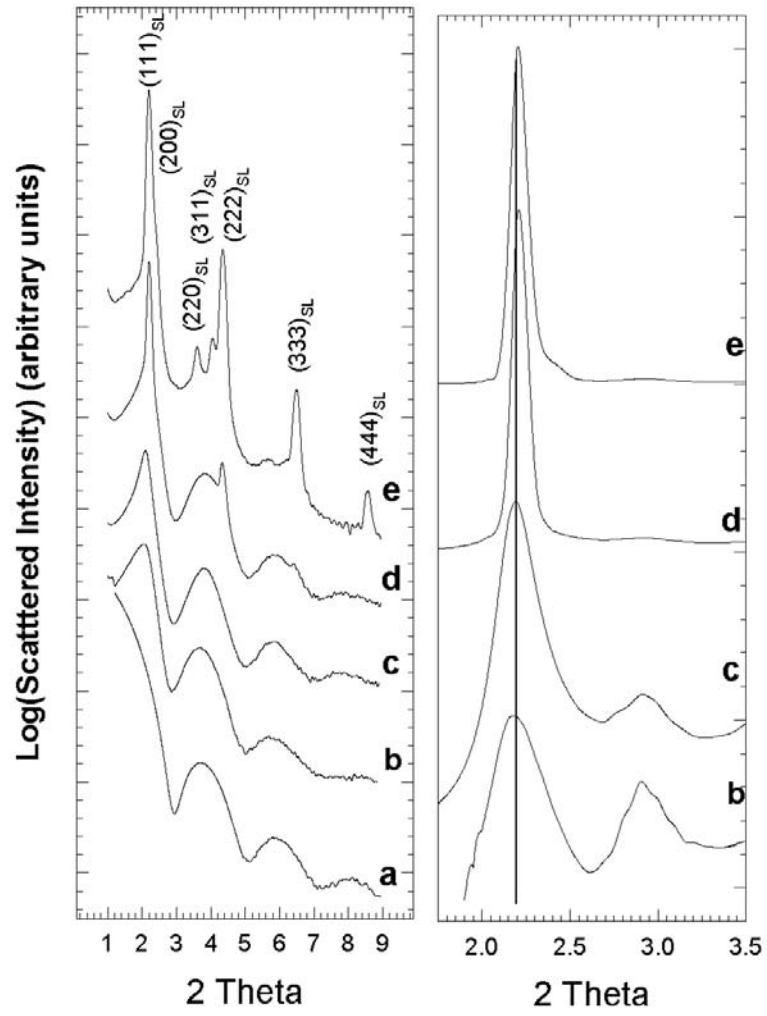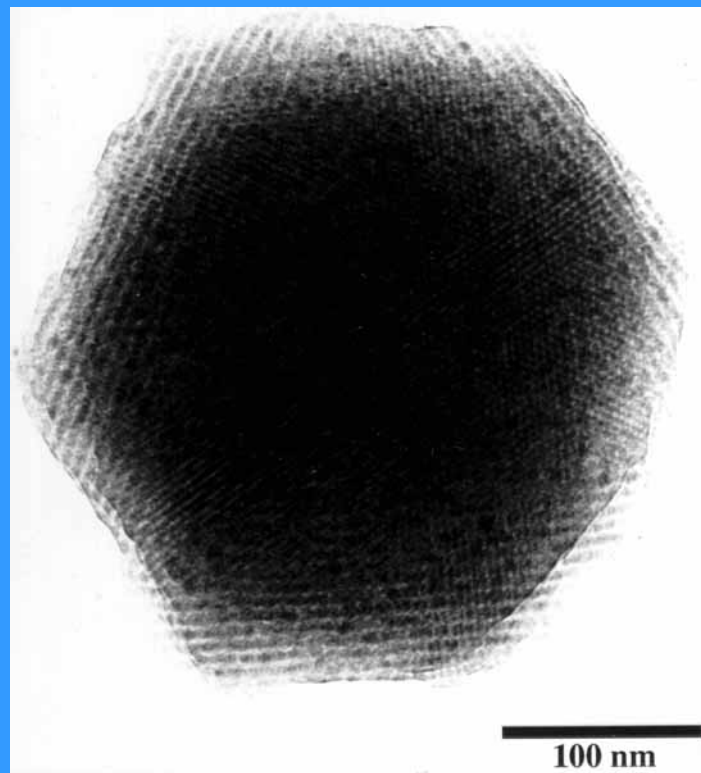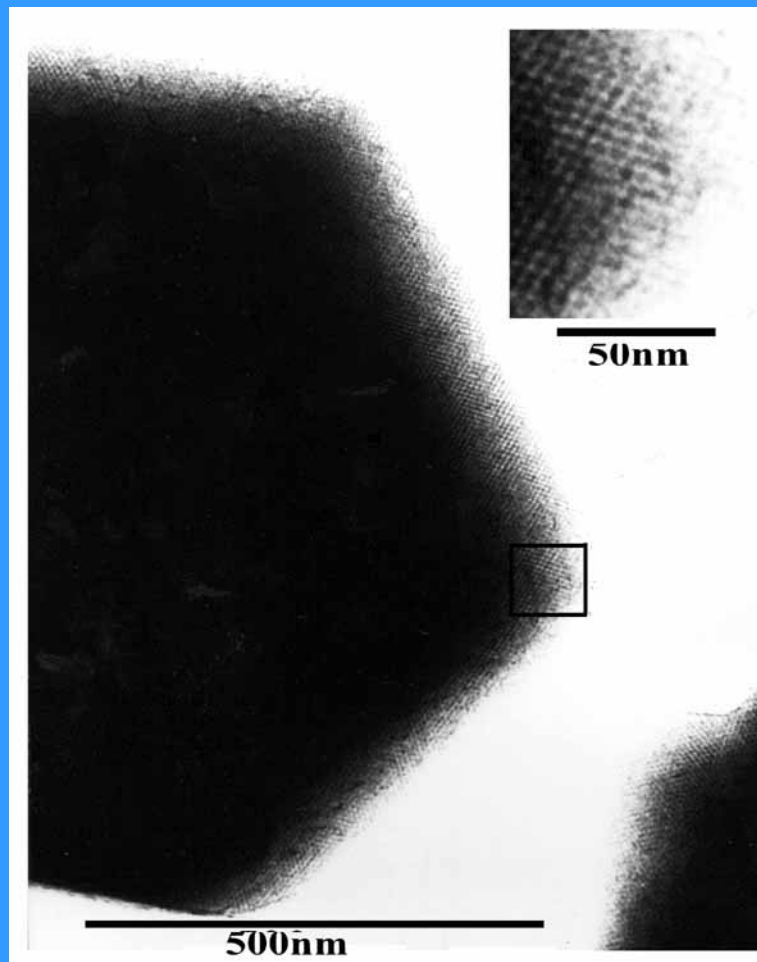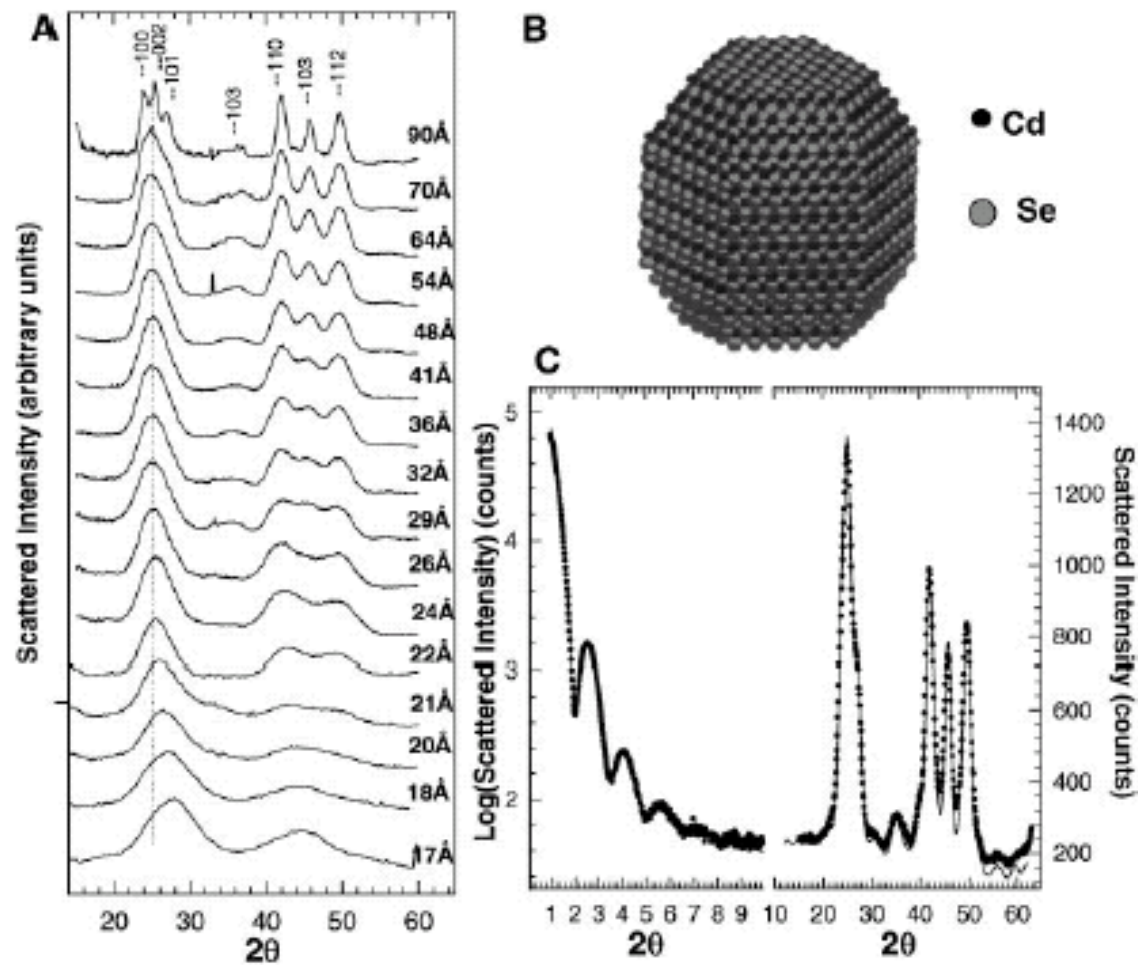
Figure 5 (*A*) WAXS patterns for CdSe NC samples ranging from 17 to 90 Å in diameter. (*B*) Three-dimensional representation of a CdSe NC, as developed from TEM studies, exemplifies the atomistic structure employed in SAXS and WAXS modeling (62). (*C*) SAXS and WAXS pattern for an ~4500 atom (62 Å) CdSe NC samples (dots). Simultaneous fitting, using nonlinear least squares methods, to the SAXS and WAXS patterns fits the sample average NC size to ~4500 atoms, aspect ratio to 1.2 (prolate), and size distribution to 4.2%.

Modeling Stacking faults

Modeling NP Shape
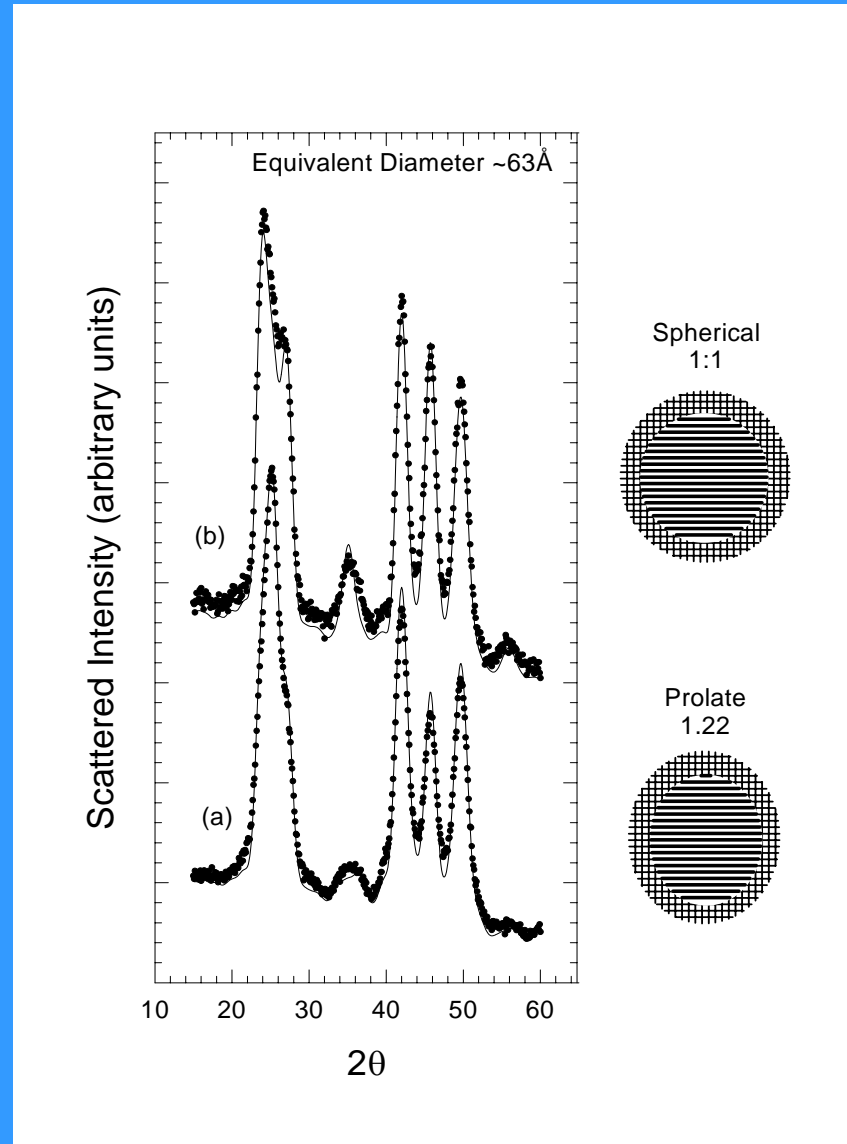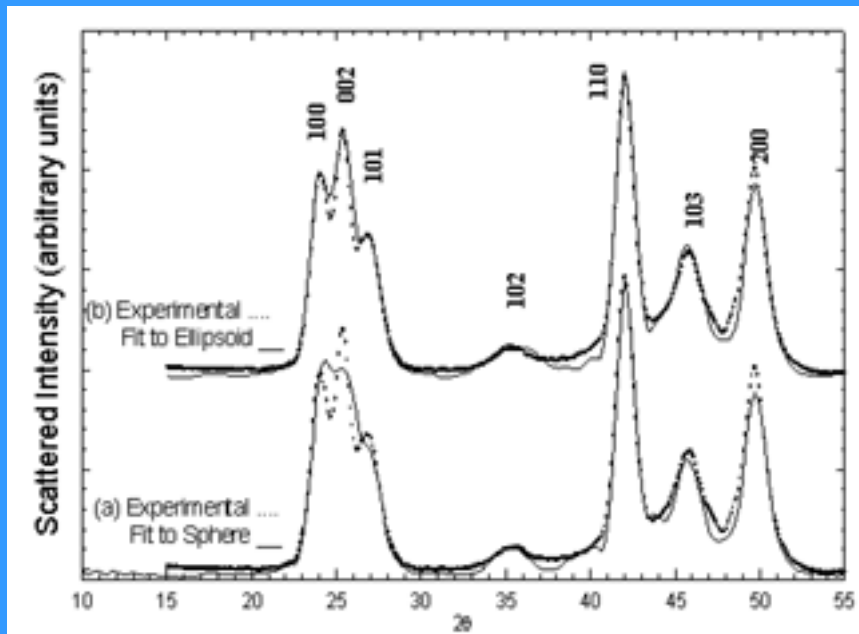
Small angle X-ray Scattering SAXS
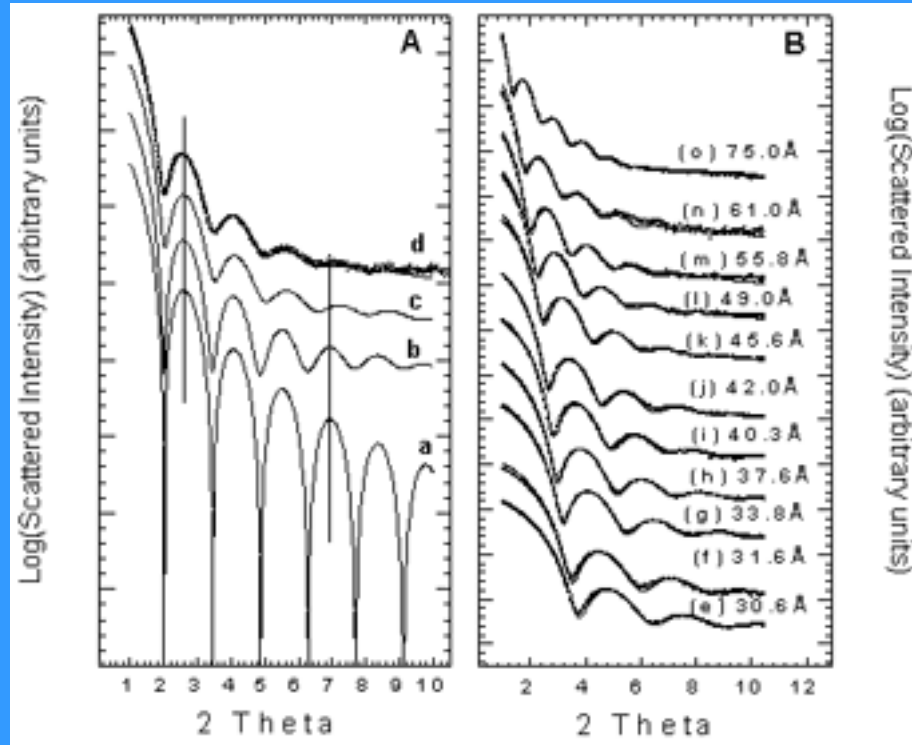
(4.8) $I(q) = I_o N[(\rho - \rho_o)^2 \frac{4}{3} \pi R^3 [3 \frac{\sin(qR) - qR\cos(qR)}{(qR)^3}]]^2$

Where ρ and ρ_o are the electron density of the particle and the dispersing medium respectively. I_o is the incident intensity and N is the number of particles. F(q) is the material form factor (the fourier transform of the shape of the scattering object) and is the origin of the oscillations observed. Thus for a spherical particle of radius R

(4.9) $I(q) = I_o N(\rho - \rho_o)^2 F^2(q)$

(4.10) $F(q) = \frac{4}{3} \pi R^3 [3 \frac{\sin(qR) - qR\cos(qR)}{(qR)^3}]$

The scattered intensity, $I(q)_{total}$, from an arbitrary collection of N particles is

$$I(q)_{total} = I_o N F^2(q) S(q), \qquad 5.$$

where the structure factor $S(q)$ is the interference introduced by the correlation between particle positions. The structure factor can be extracted from the experimental data by dividing the SAXS pattern of the NC glasses by that of the NCs dispersed in PVB. When the NCs are dilute, their positions are uncorrelated and $S(q) \sim 1$. Equation 6 expresses the structure factor in terms of an average radial distribution $\rho(r)$ of particles about an arbitrary reference particle (110).
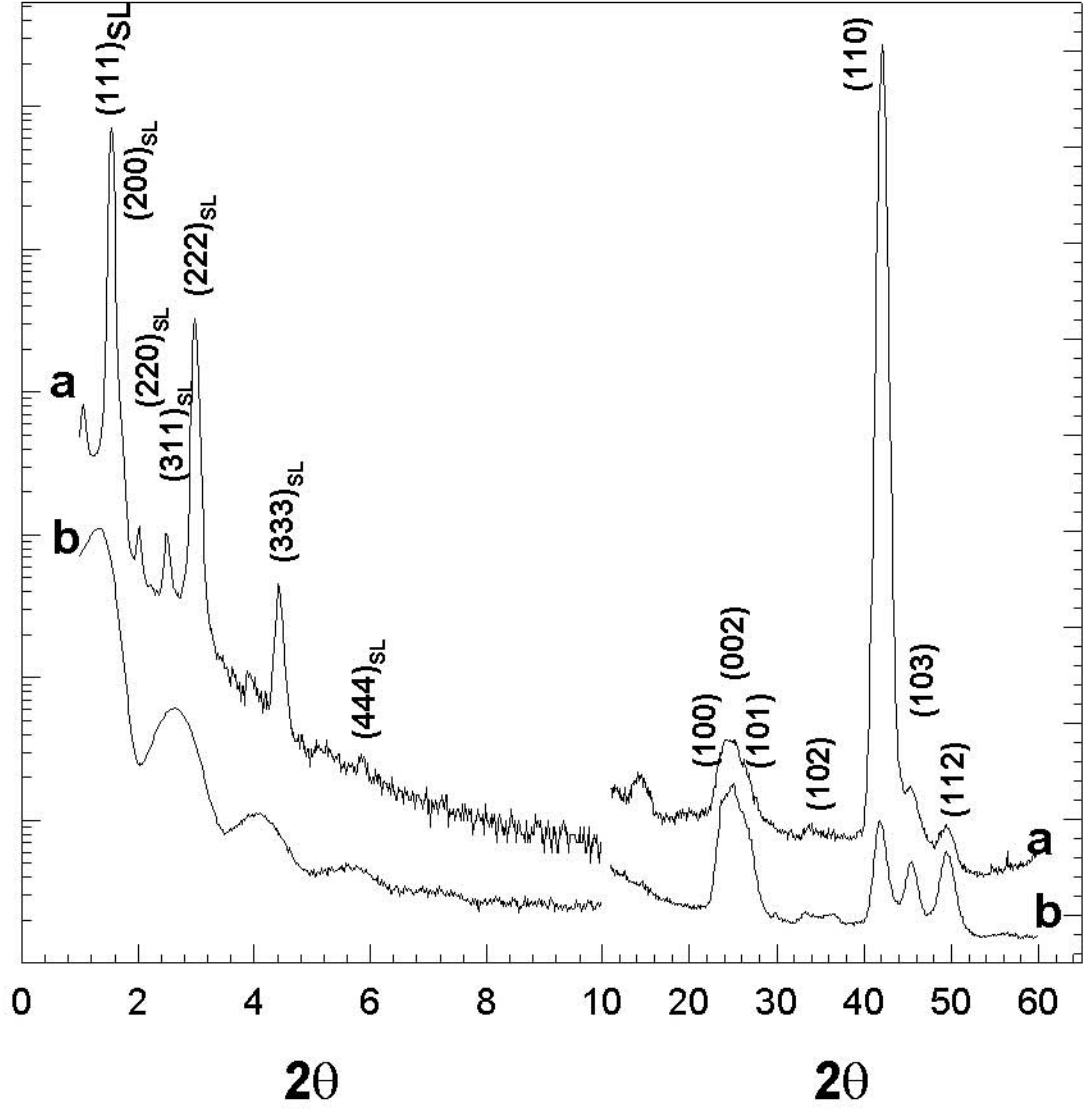
$$S(q) = 1 + \frac{4\pi\rho_0}{q} \int_0^\infty r \left[\frac{\rho(r)}{\rho_0} - 1 \right] \sin(qr)\, dr \qquad 6.$$

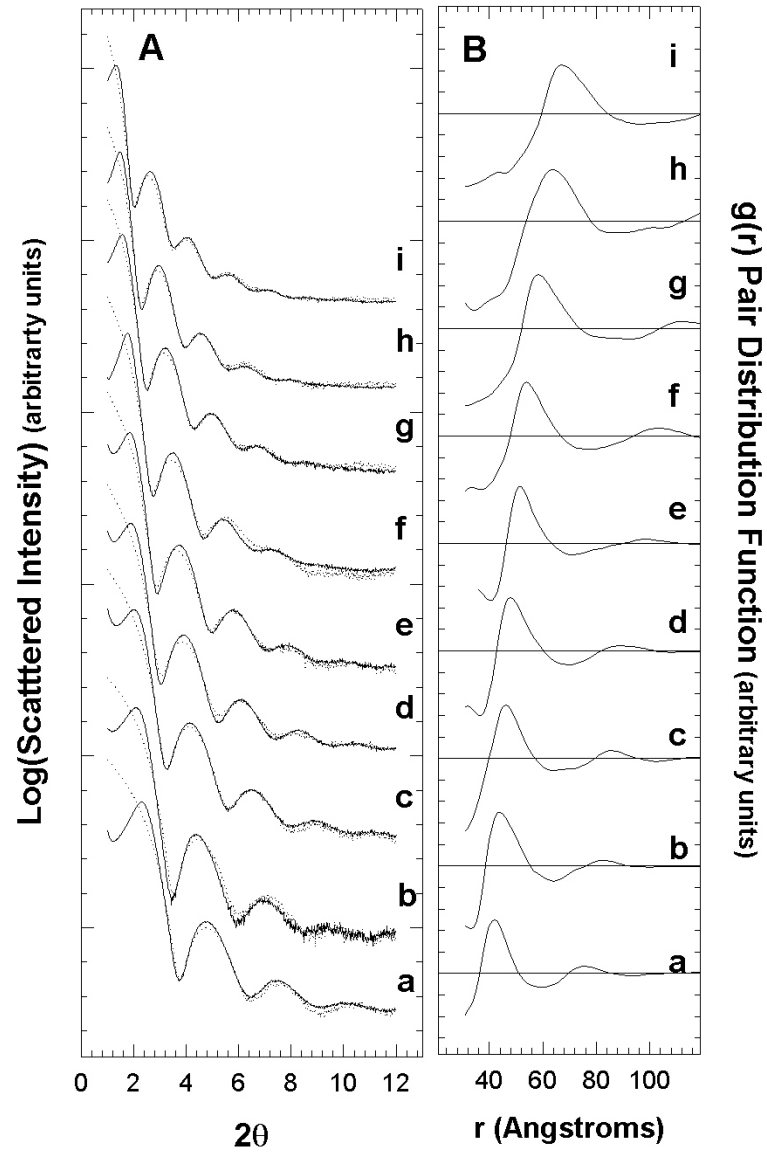The structure factor can be Fourier transformed to yield a pair distribution function (PDF) $g(r)$ where

$$g(r) = \frac{\rho(r)}{\rho_0} = 1 + \frac{1}{2\pi^2 r \rho_0} \int_0^\infty [S(q) - 1] q \sin(qr)\, dq. \qquad 7.$$
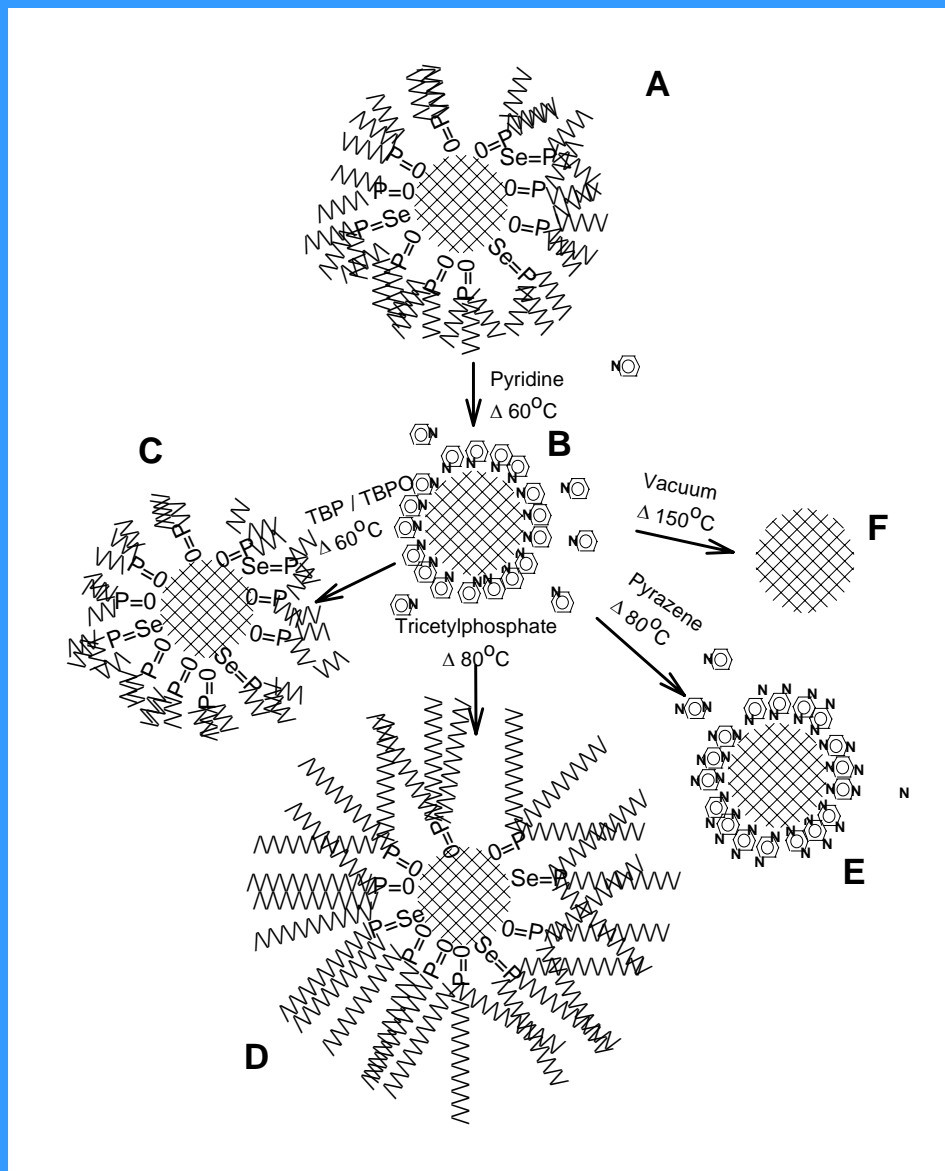
A

i

h

g

f

e

d

c

b

a

Log(Scatttered Intensity) (arbitrarty units)

0   2   4   6   8   10   12

2θ

B

i

h

g

f

e

d

c

b

a

g(r) Pair Distribution Function (arbitrary units)

40   60   80   100

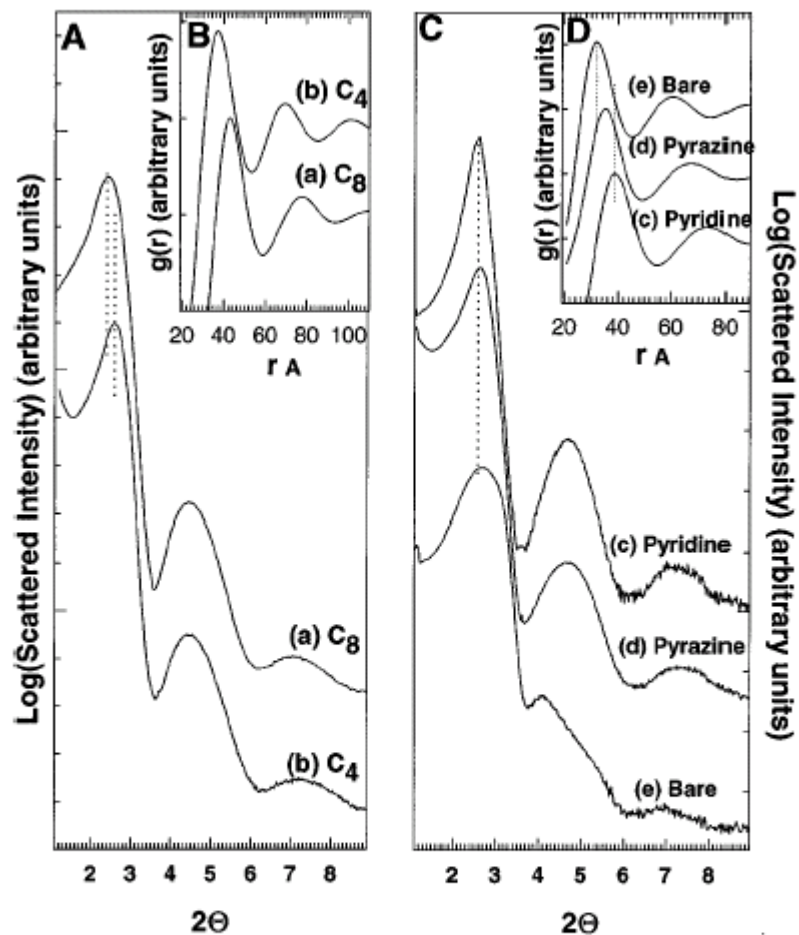**r (Angstroms)**

Cap exchange to modify surface:

Figure 11 (*A*) SAXS patterns for close-packed glassy solids of 32 Å NCs with (a) TOPO caps and (b) TBPO caps. Inset (*B*) PDFs gives inter-particle separations for (a) of 11 Å and (b) or 7 Å. (C) SAXS patterns for glassy solids of 34 Å CdSe NCs capped with (c) pyridine, (d) pyrazine, and (e) bare semiconductor surfaces. Inset (*D*) PDFs give inter-particle spacings of (c) 7 Å, (d) 5 Å, and (e) <2 Å.
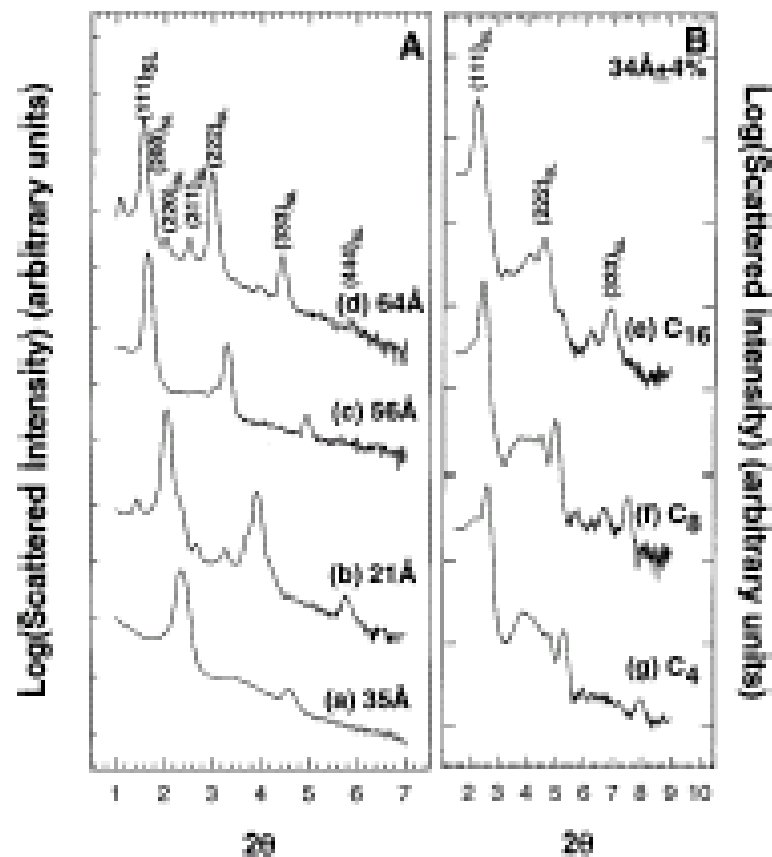
Figure 21 (A) SAXS patterns for epitaxial superlattices prepared from CdSe NCs ranging from 35 to 64 Å in diameter. The fcc superlattice reflections are indicated for the 64 Å CdSe NC superlattice. (B) SAXS patterns of ordered epitaxial thin films prepared from 34 Å CdSe NCs derivatized with (e) trioctylphosphate, giving a ~17 Å inter-particle spacing; with (f) the native trioctylphosphine chalcogenide, giving a ~11 Å spacing; and with (g) tributylphosphine oxide, giving a ~7 Å spacing (45).

TEM image of a 3D superlattice formed by **nanospheres** with **hexagonal symmetry**. Inset: Wide angle electron diffraction pattern indicates directional ordering (see arrow)
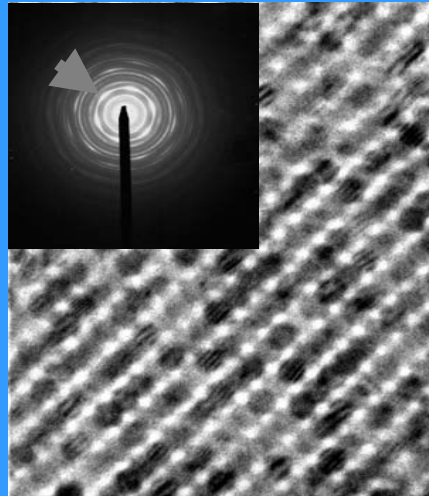
TEM image of a superlattice formed by **nanocubes**. Inset: Electron diffraction pattern of a 3D superlattice showing directional ordering. The superlattice shows **cubic symmetry.**
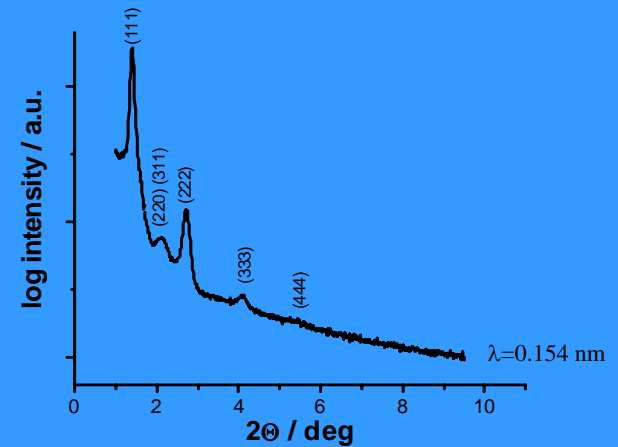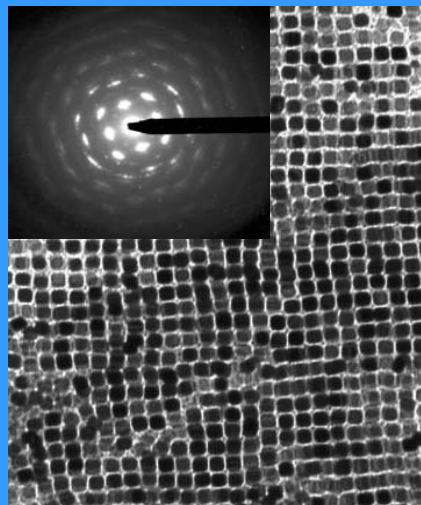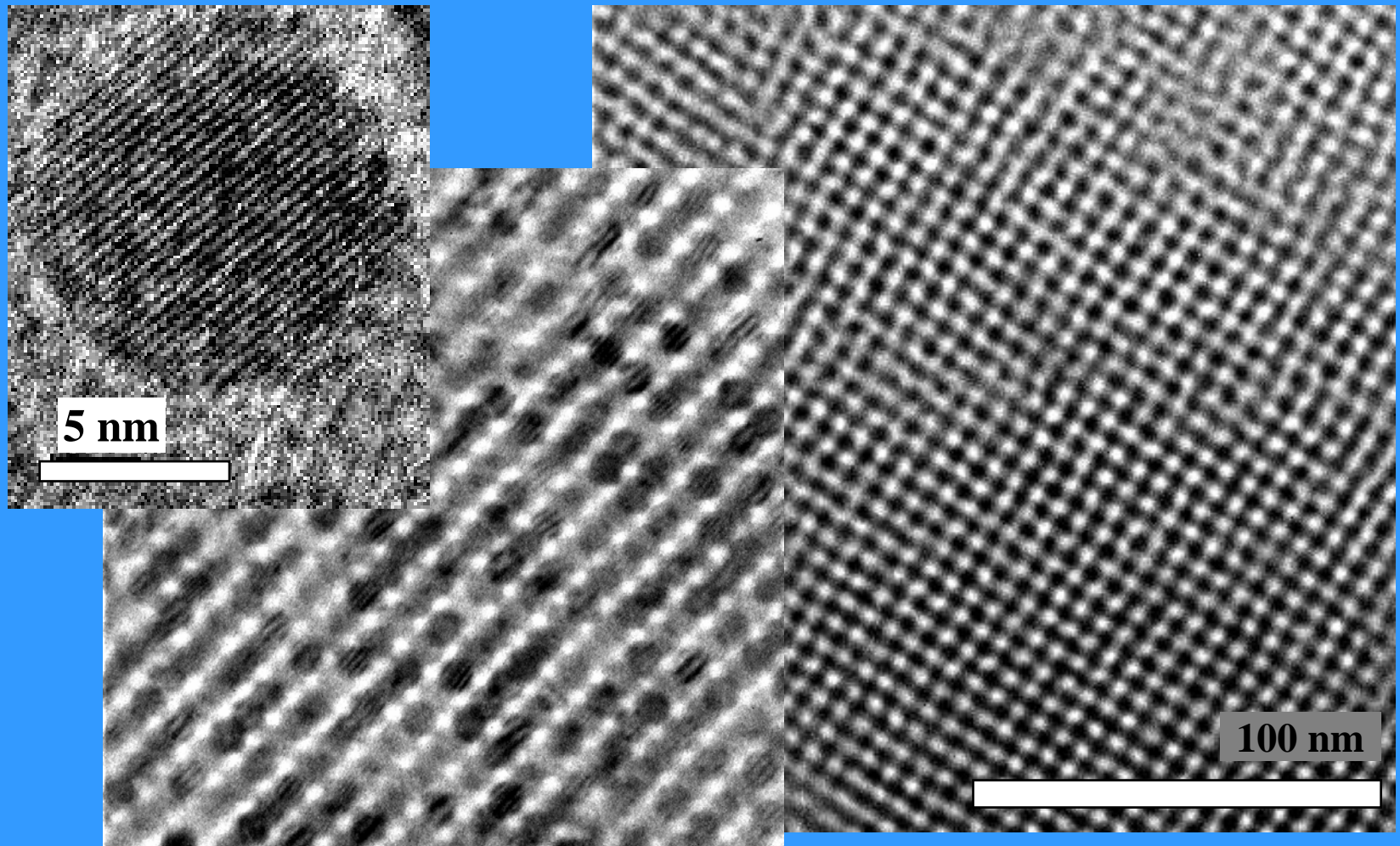

Small angle X-ray (SAXS) reflections for a fcc superlattice formed by **spheres**
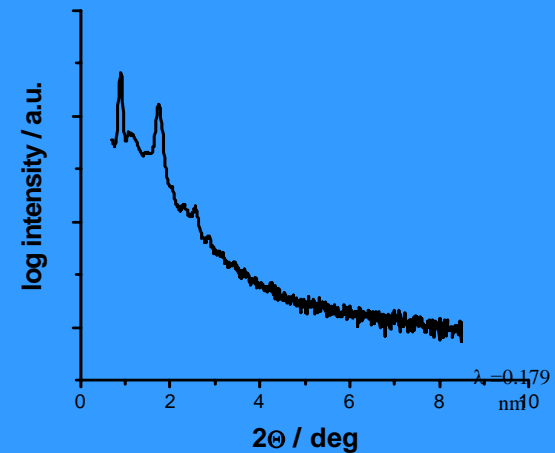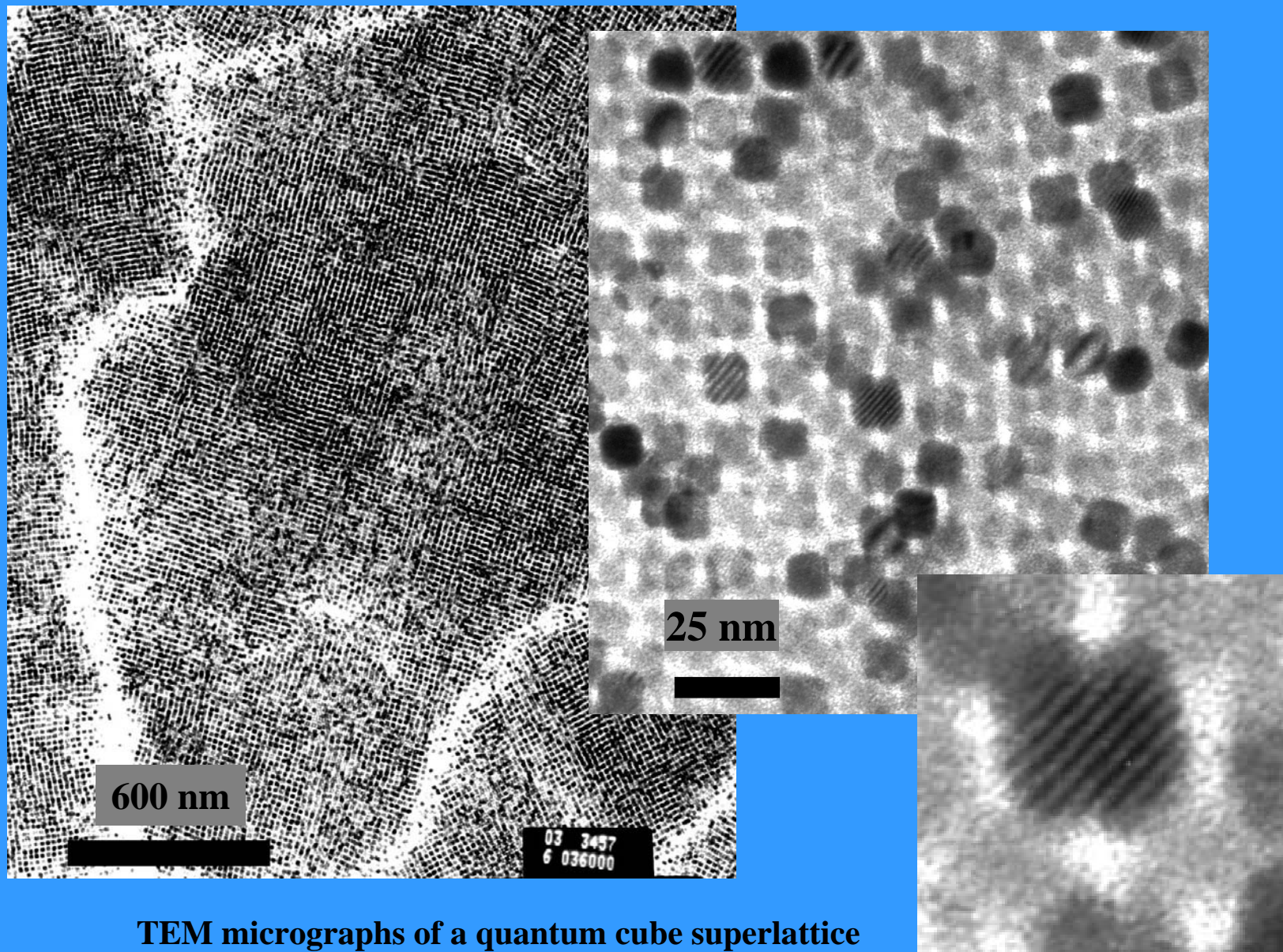
SAXS of a superlattice formed by **cubes**

**TEM micrographs of a fcc superlattice showing the (112) projection (left)
and the (100) projection (right)**

600 nm

25 nm

03 3457
6 036000

TEM micrographs of a quantum cube superlattice
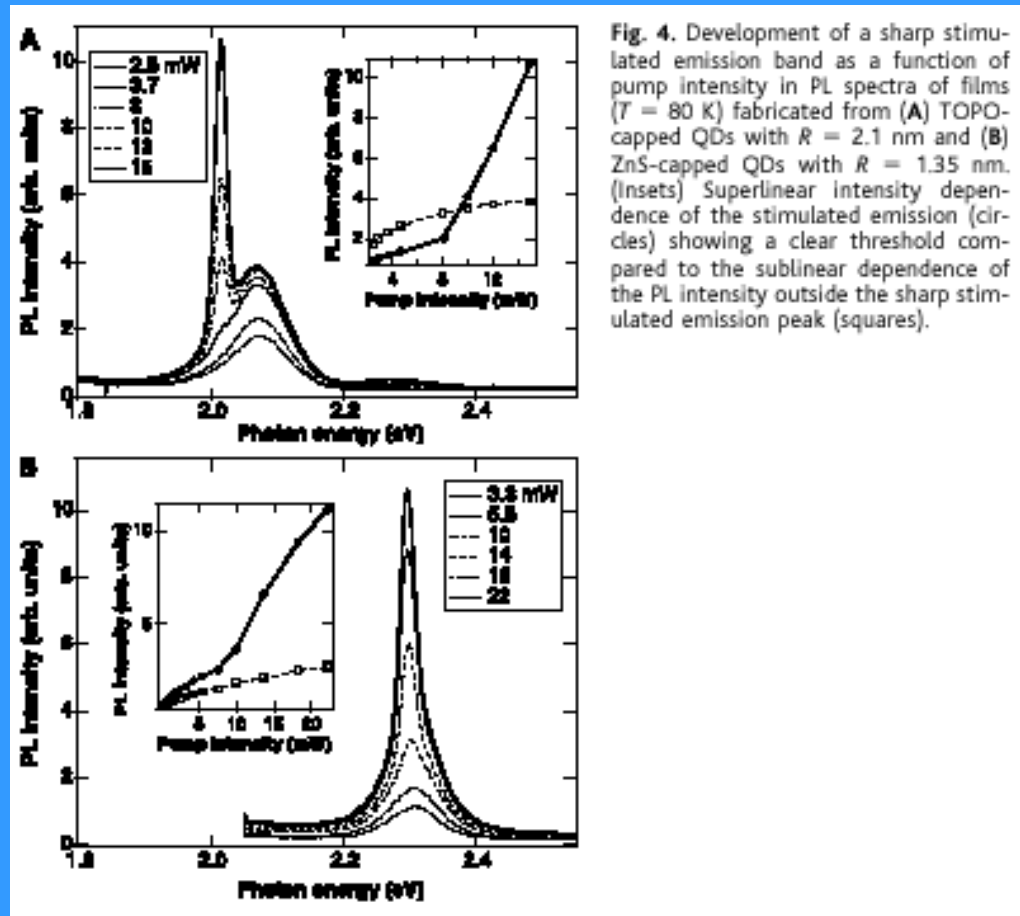
Quantum Dot Solids for Amplified Stimulated Emission

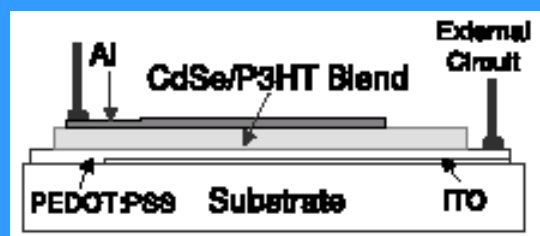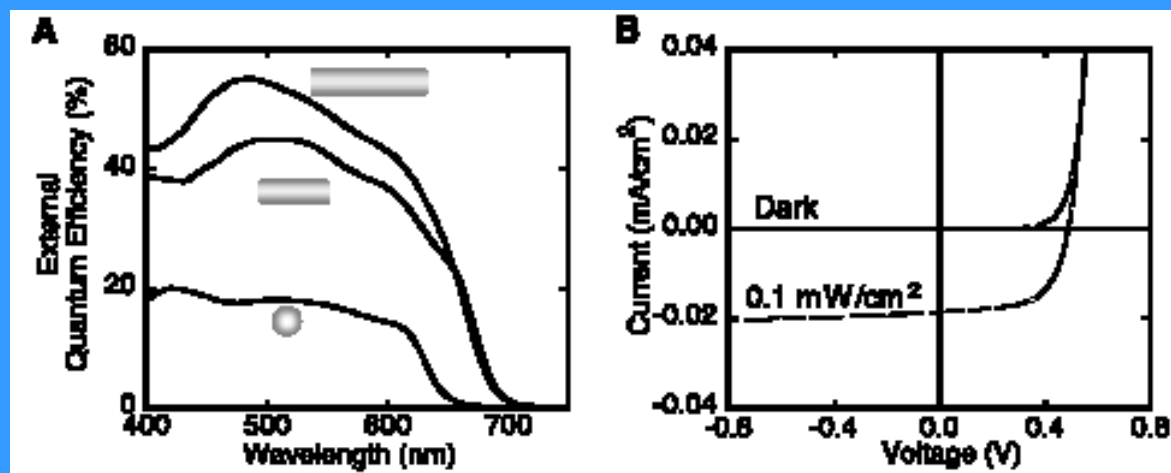

Fig. 4. Development of a sharp stimulated emission band as a function of pump intensity in PL spectra of films (T = 80 K) fabricated from (A) TOPO-capped QDs with R = 2.1 nm and (B) ZnS–capped QDs with R = 1.35 nm. (Insets) Superlinear intensity dependence of the stimulated emission (circles) showing a clear threshold compared to the sublinear dependence of the PL intensity outside the sharp stimulated emission peak (squares).

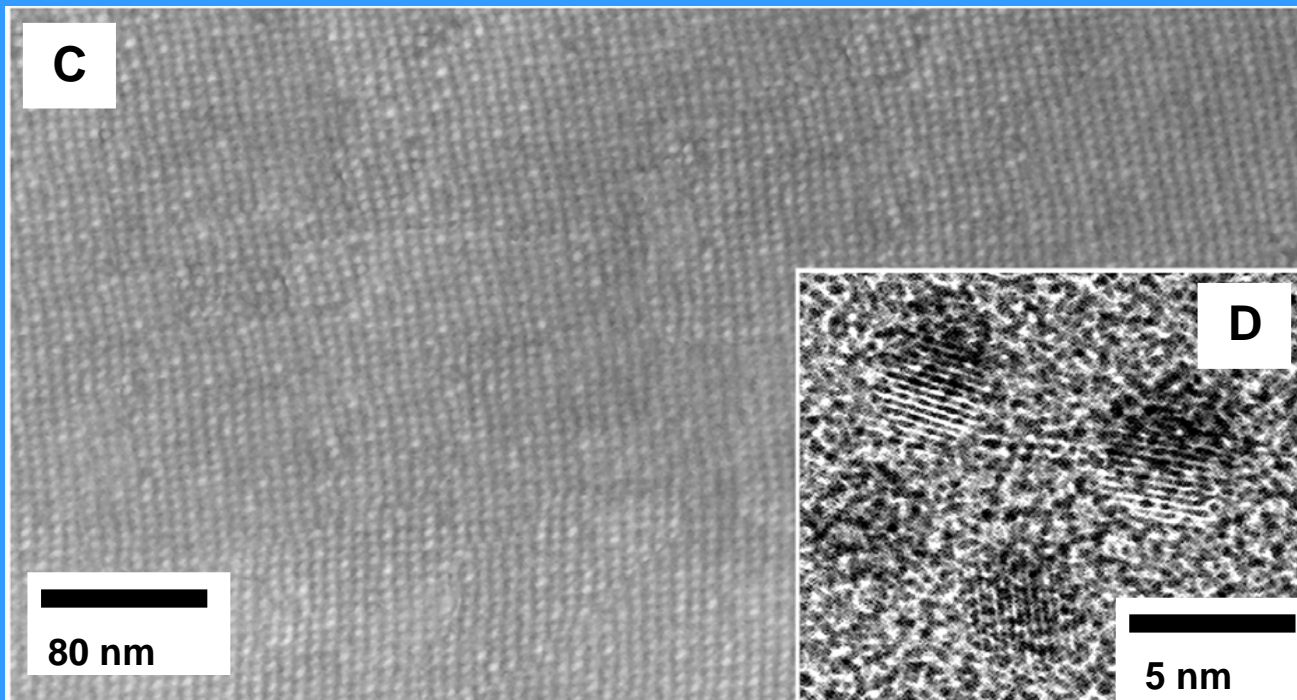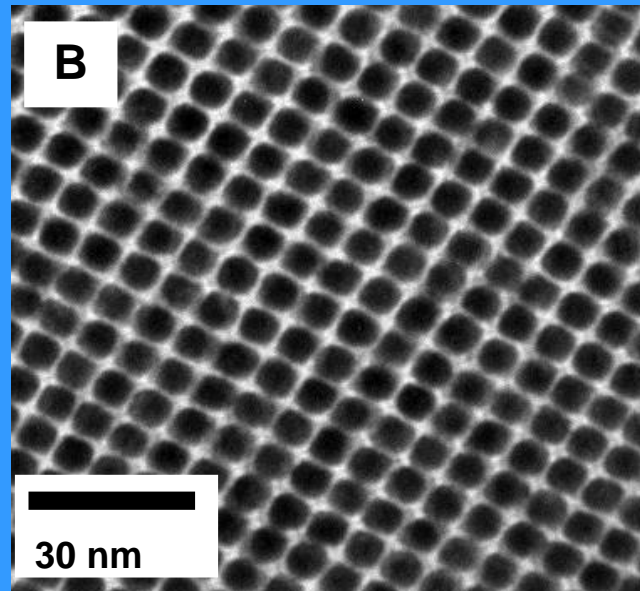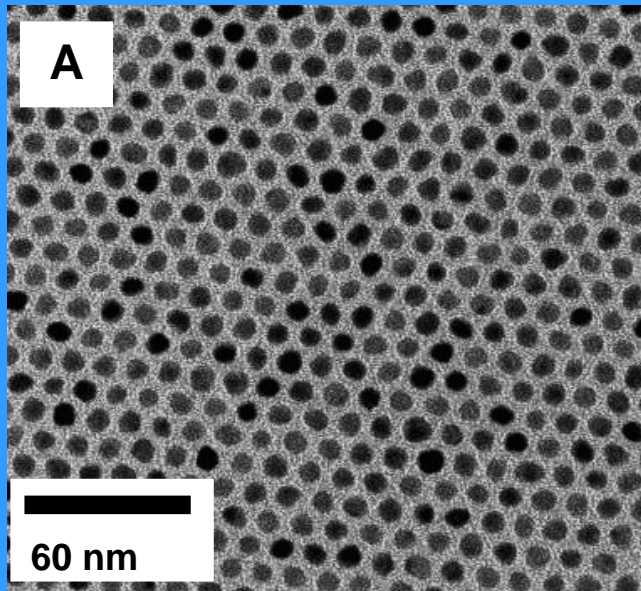V. I. Klimov, A. A. Mikhailovsky, Su Xu, A. Malko, J. A. Hollingsworth, C. A. Leatherdale, H.-J. Eisler, M. G. Bawendi, Science, **290**, 314 (2000).
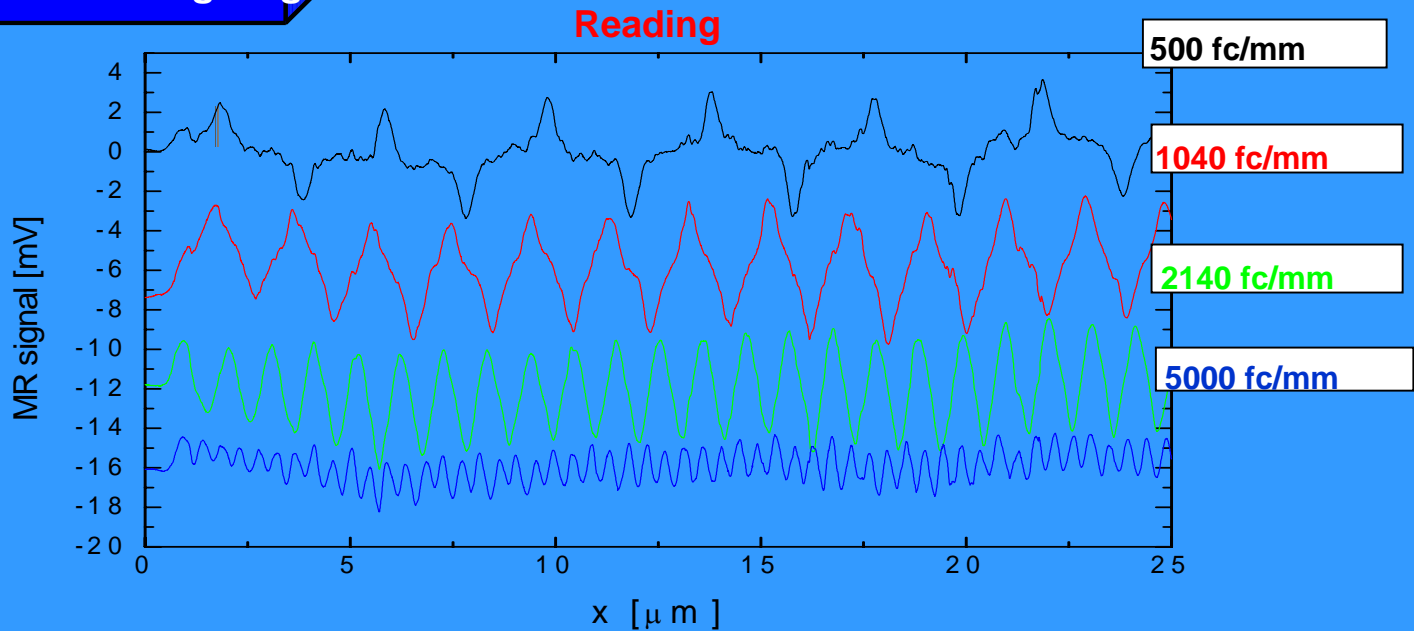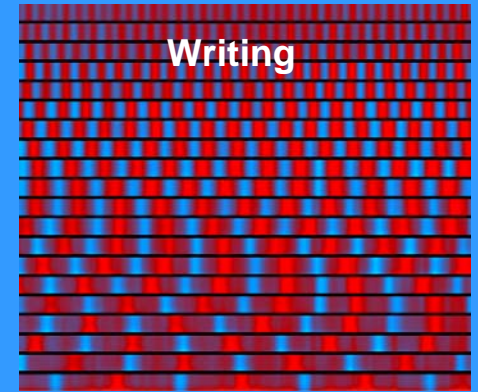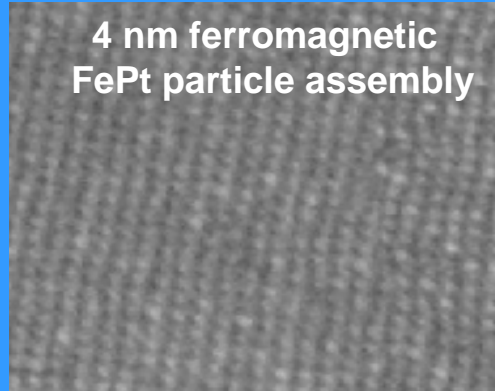
Quantum Dot Solar Cells

90 wt% QDs

FePt Nanocrystals (4 nm)

Magnetic recording

Computer V → I

Servo Electronics

to piezos

Suspension

Slider

Sample

X-Y Piezo Scanning Stage

4 nm ferromagnetic FePt particle assembly

Writing

Reading

MR signal [mV]

500 fc/mm

1040 fc/mm

2140 fc/mm

5000 fc/mm

x [μm]
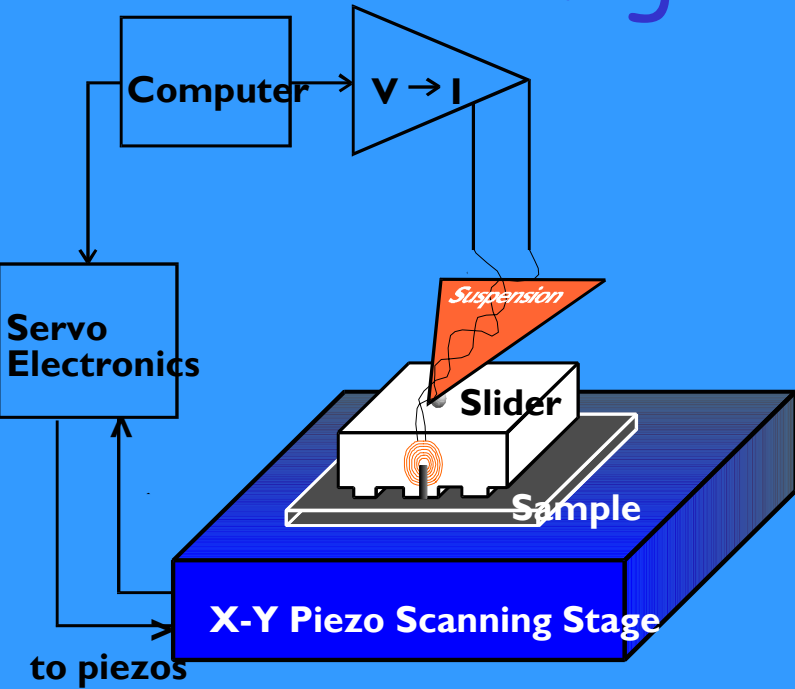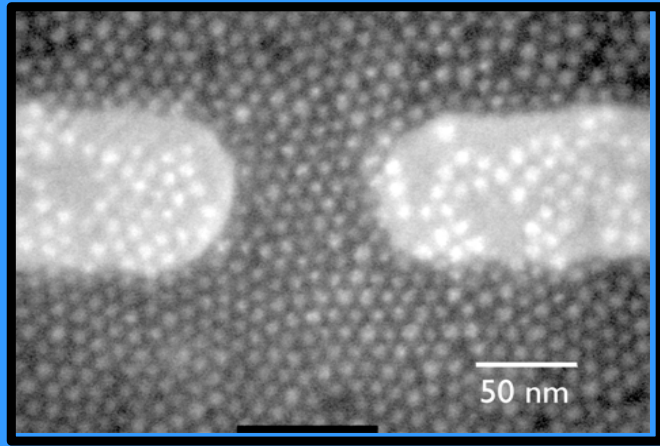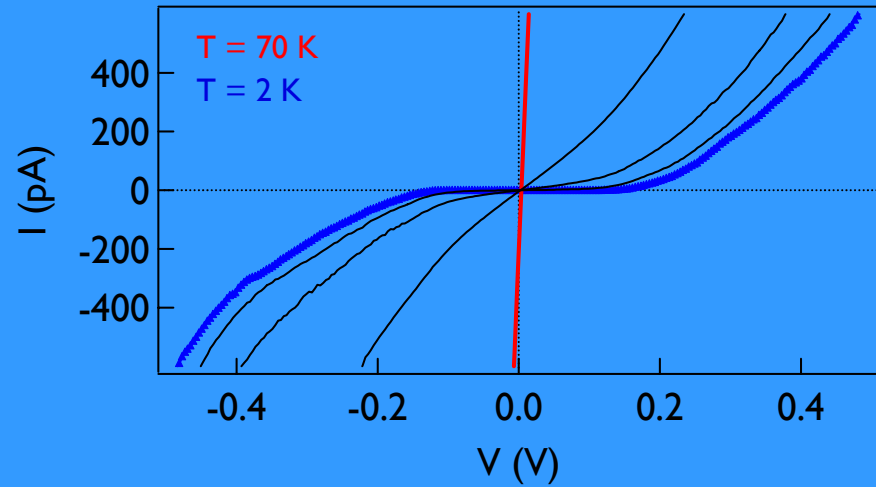
Spin-dependent tunneling in Nanocrystal arrays

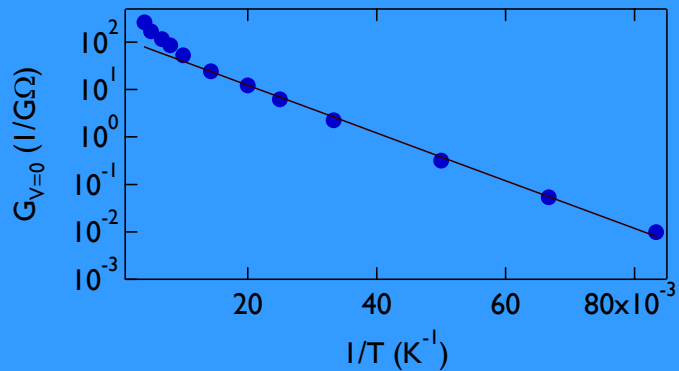Chuck Black, Bob Sandstrom, Chris Murray, Shouheng Sun
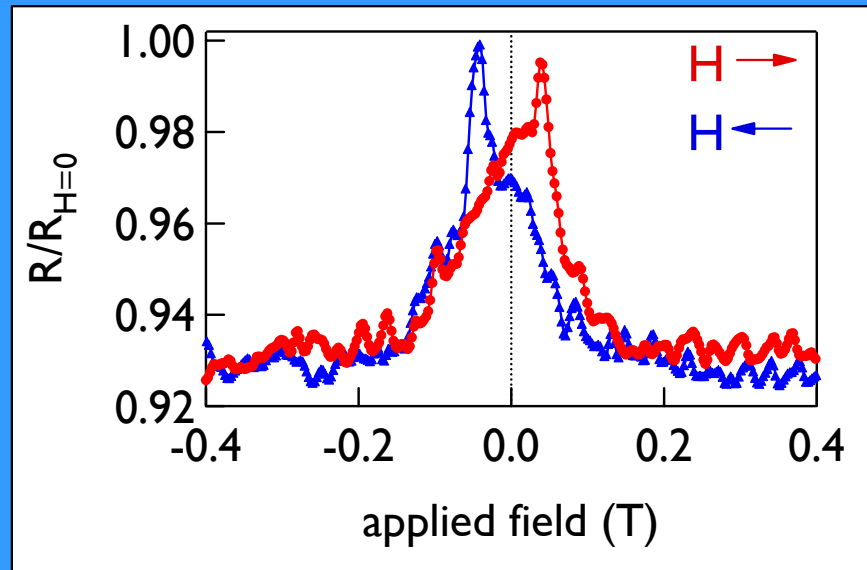

▸ shortest current path ~ 8 nanocrystals

G$_{V=0}$ follows simple thermal-activation
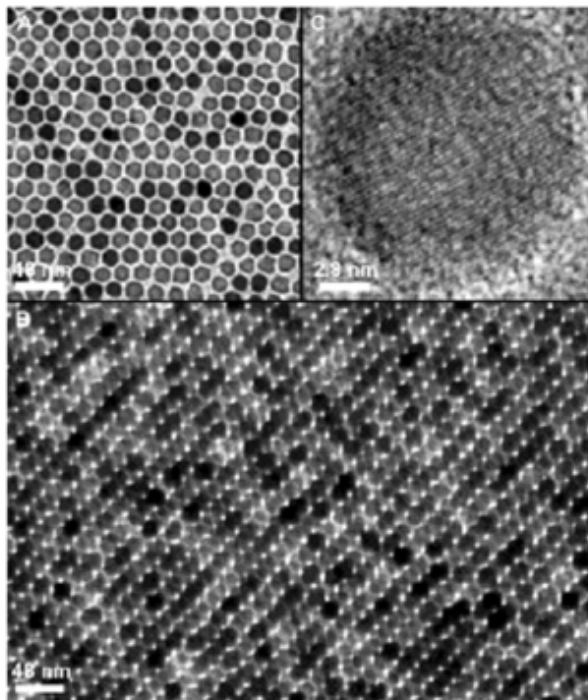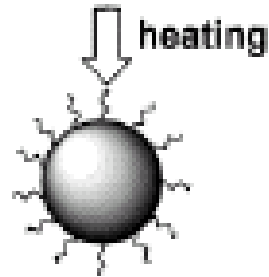

data fit by: $\ln(G_{V=0}) = \text{const.} - E_c/k_B T$

▸ from fit to data, measure $E_c \sim 10$ meV

▸ for all devices measured, 10 meV $< E_c < 14$ meV

Magnetic Nanomaterials for Functional Nanodevices

Researchers: Shouheng Sun, Hao Zeng, Min Chen

$Fe(acac)_3 + ROH + RCOOH + RNH_2 + Ph_2O$

heating

Single component Self-assembly
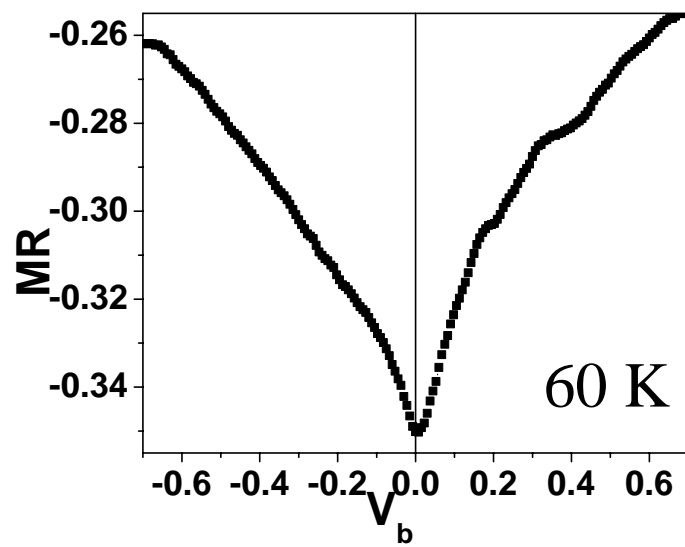
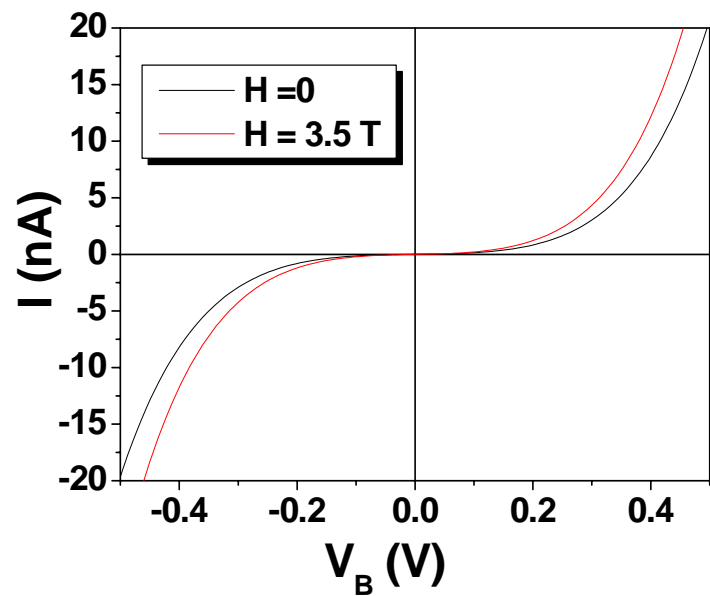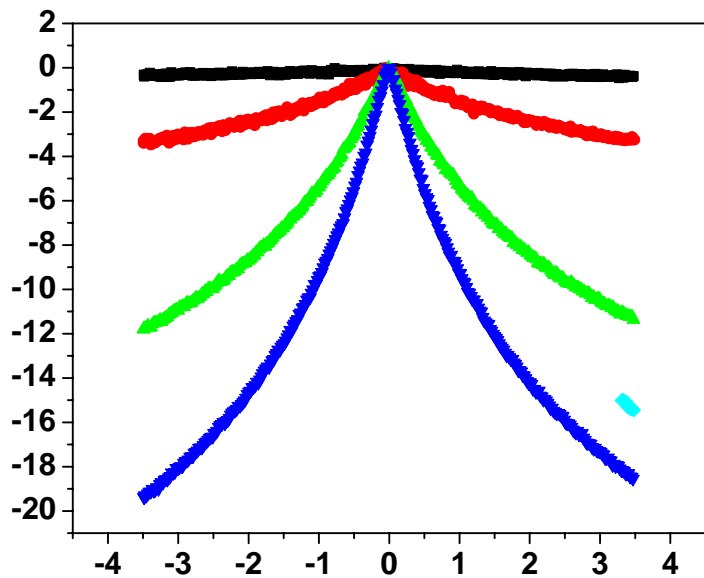Figure 1. TEM bright field image of 16-nm Fe_2O_4 nanoparticles deposited from their dodecane dispersion on amorphous carbon surface and dried at 60 °C for 30 min: (A) a monolayer assembly, (B) a multilayer assembly, (C) HRTEM image of a single Fe_2O_4 nanoparticle. The images were acquired from a Philips EM 430 at 300 KV.

50 nm
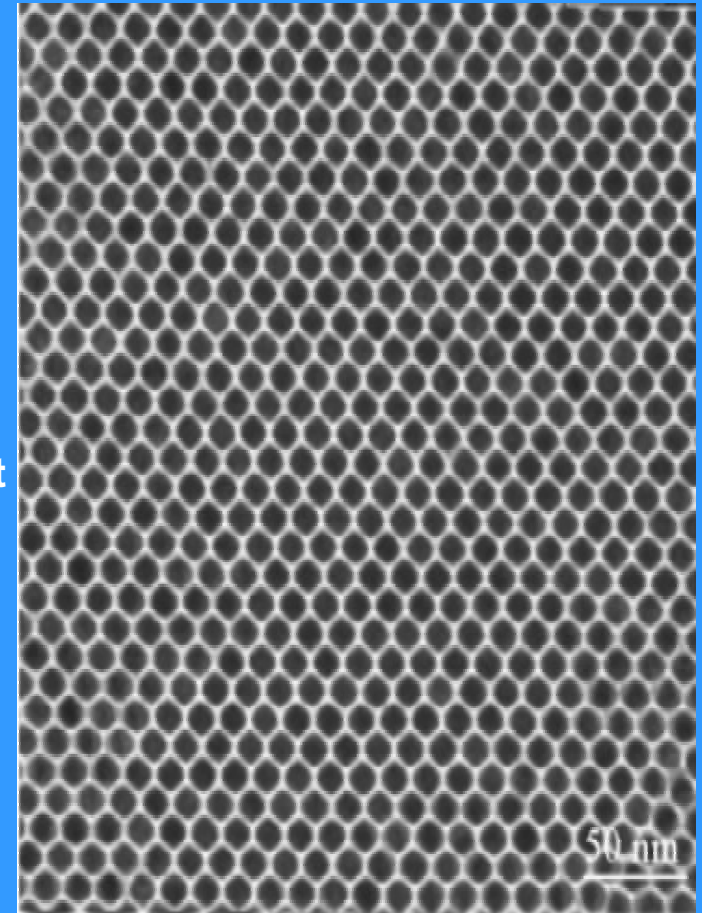
Self-assembled Fe3O4 NPs
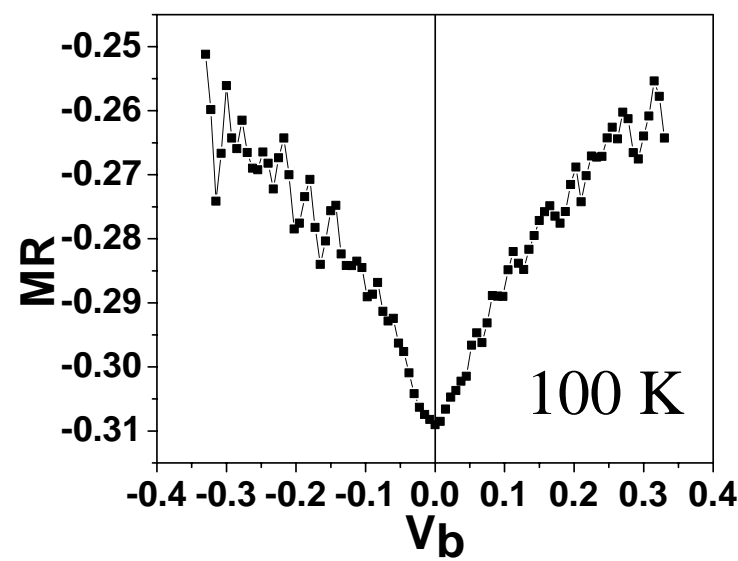
Potential for spintronic device applications

Qunatum cubes:

Cubic 12 nm PbSe nanocrystals Assembling into a superlattice.

(100) (112)

(111) (101)
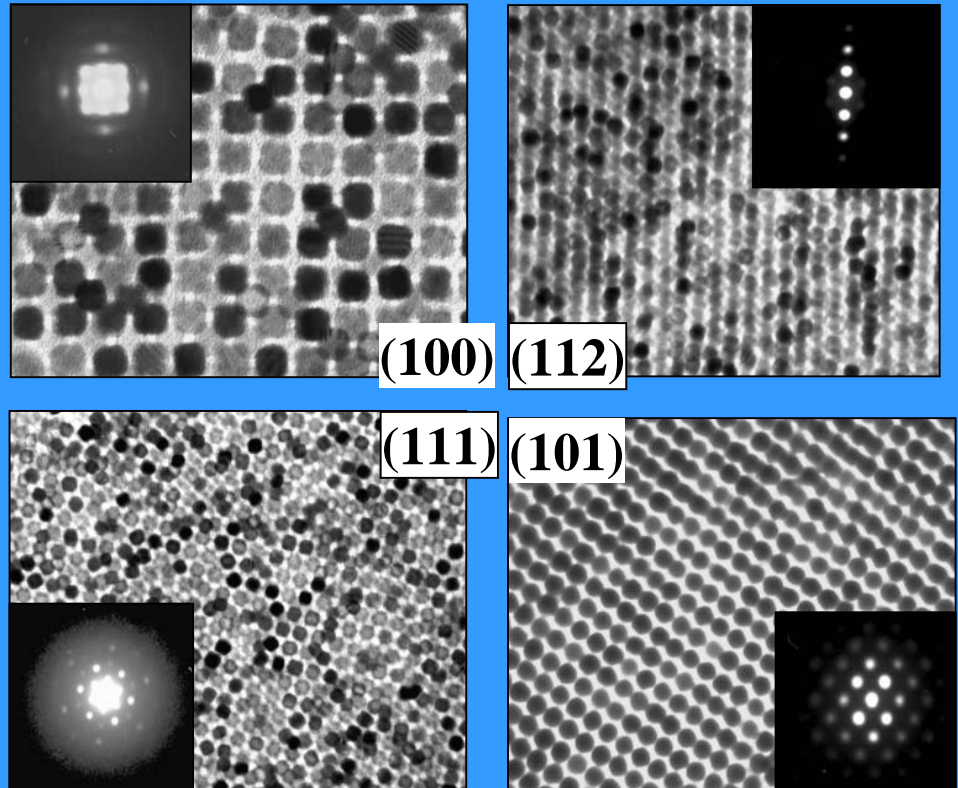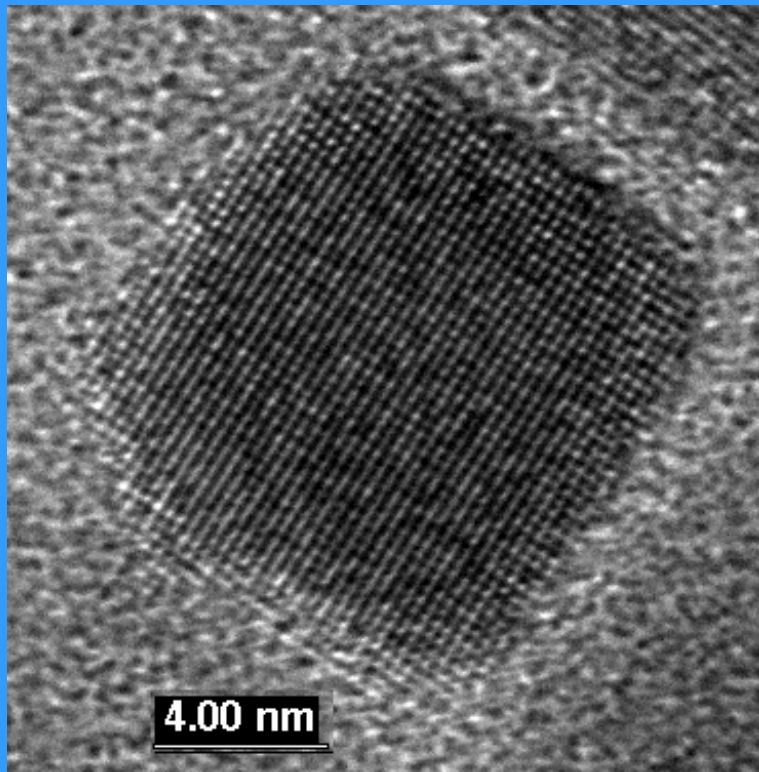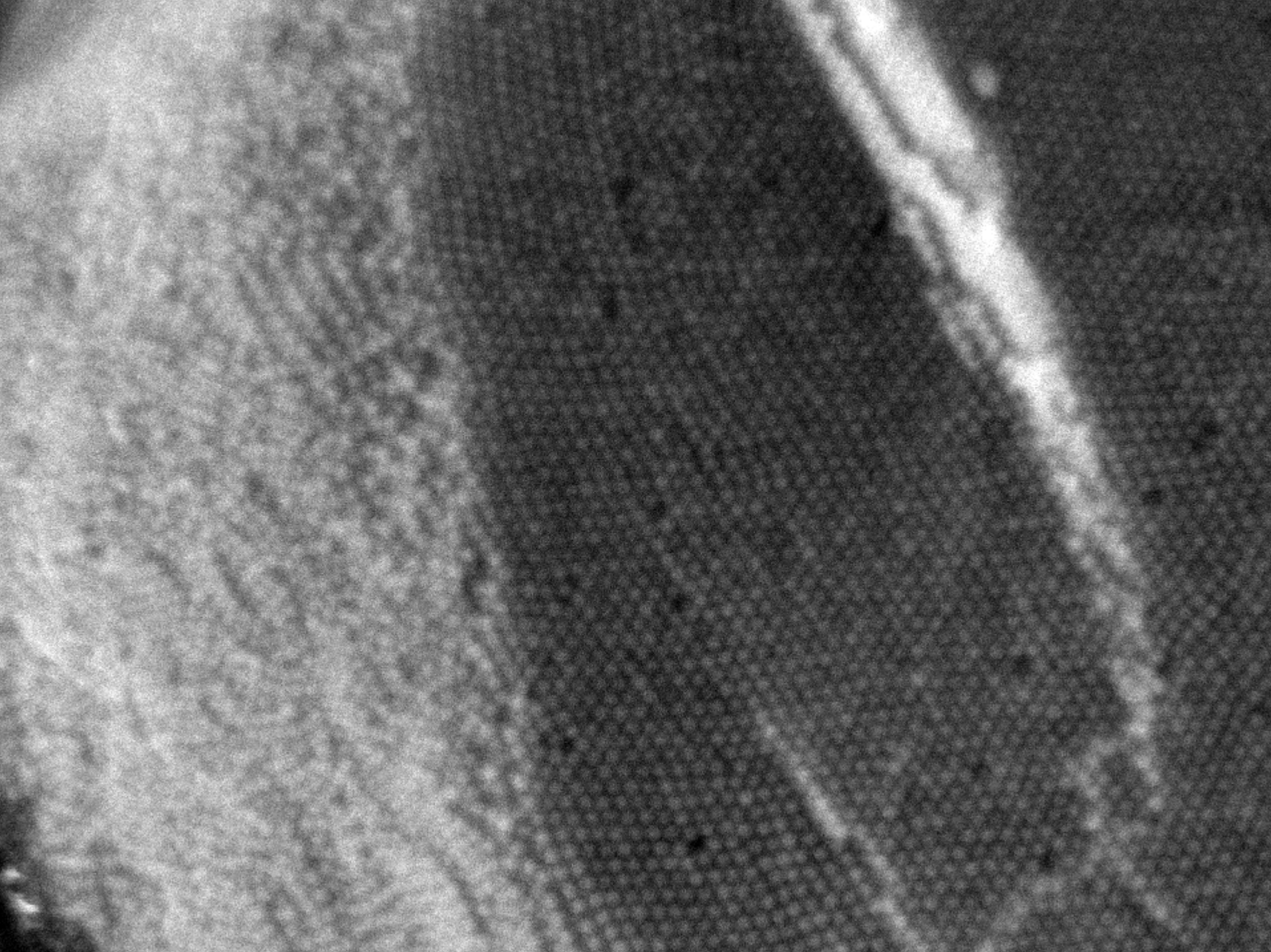
Large terrace on PbSe Superlattice of 10 nm PbSe Nanocrystals
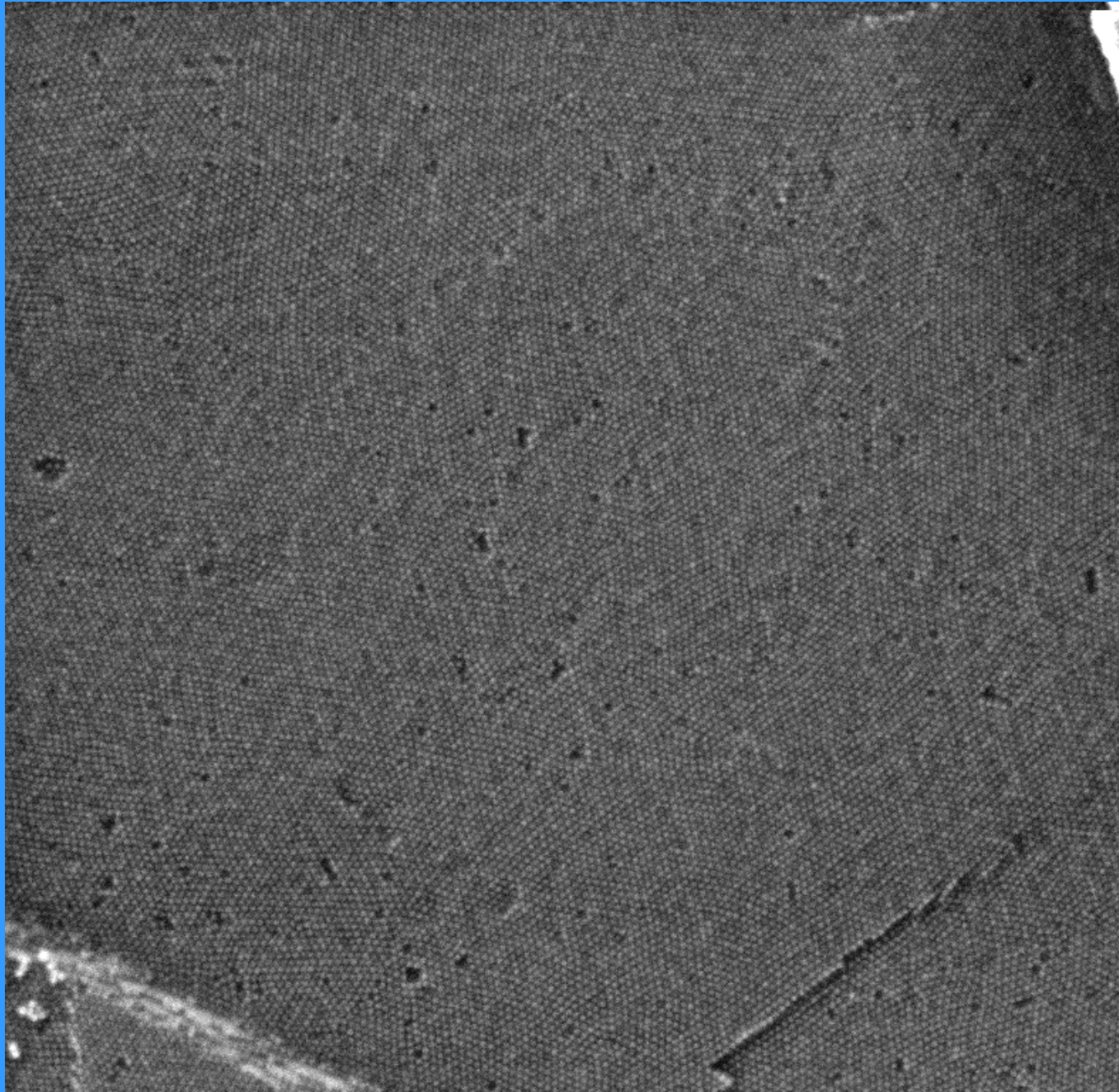
Self-assembled CdSe nanorod solids
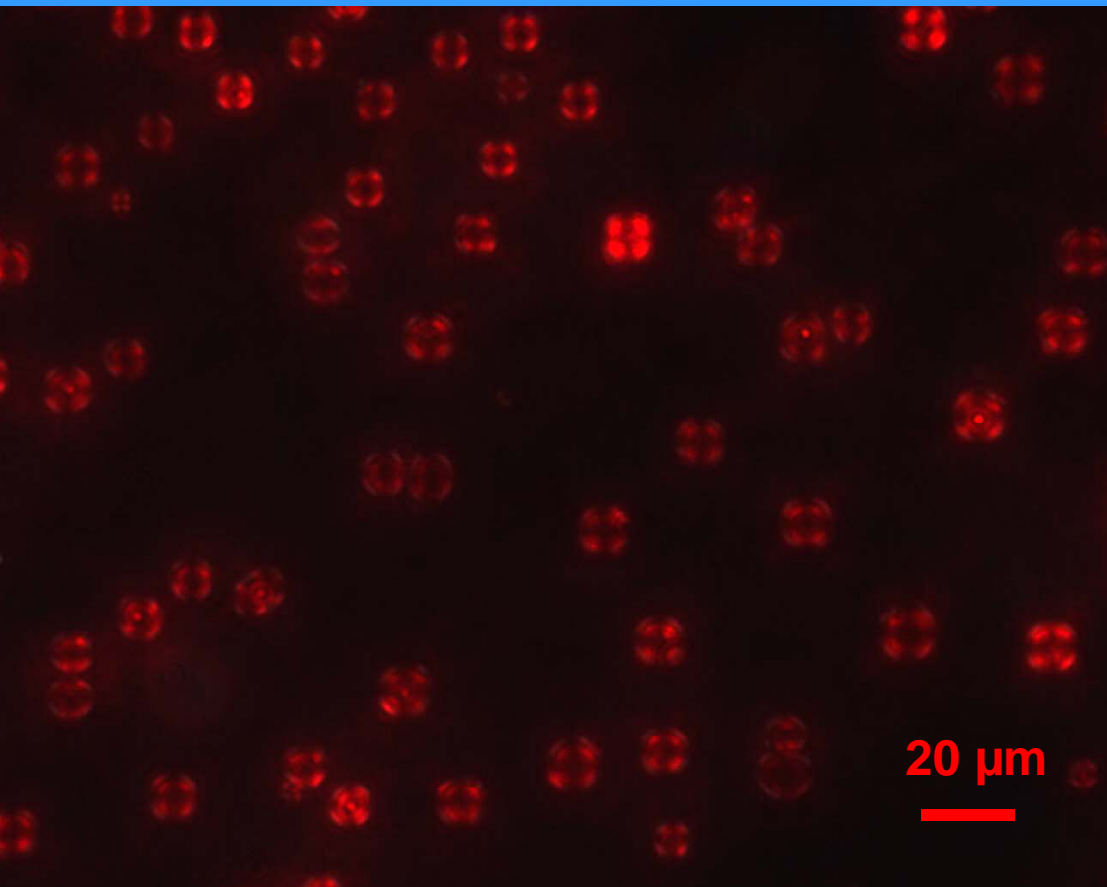
Optical micrograph of self-assembled CdSe nanorods (between crossed polarizers).

without polarizers

with crossed polarizers

20 µm

20 µm
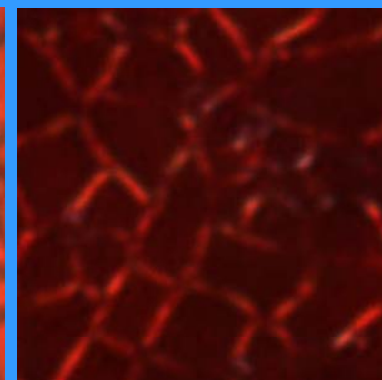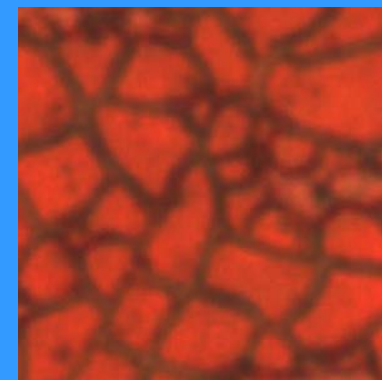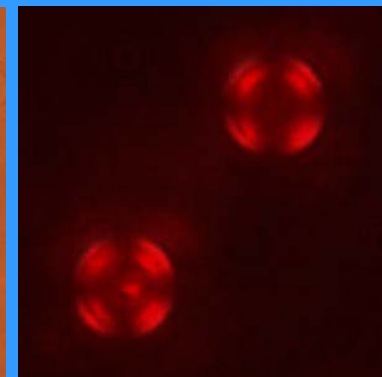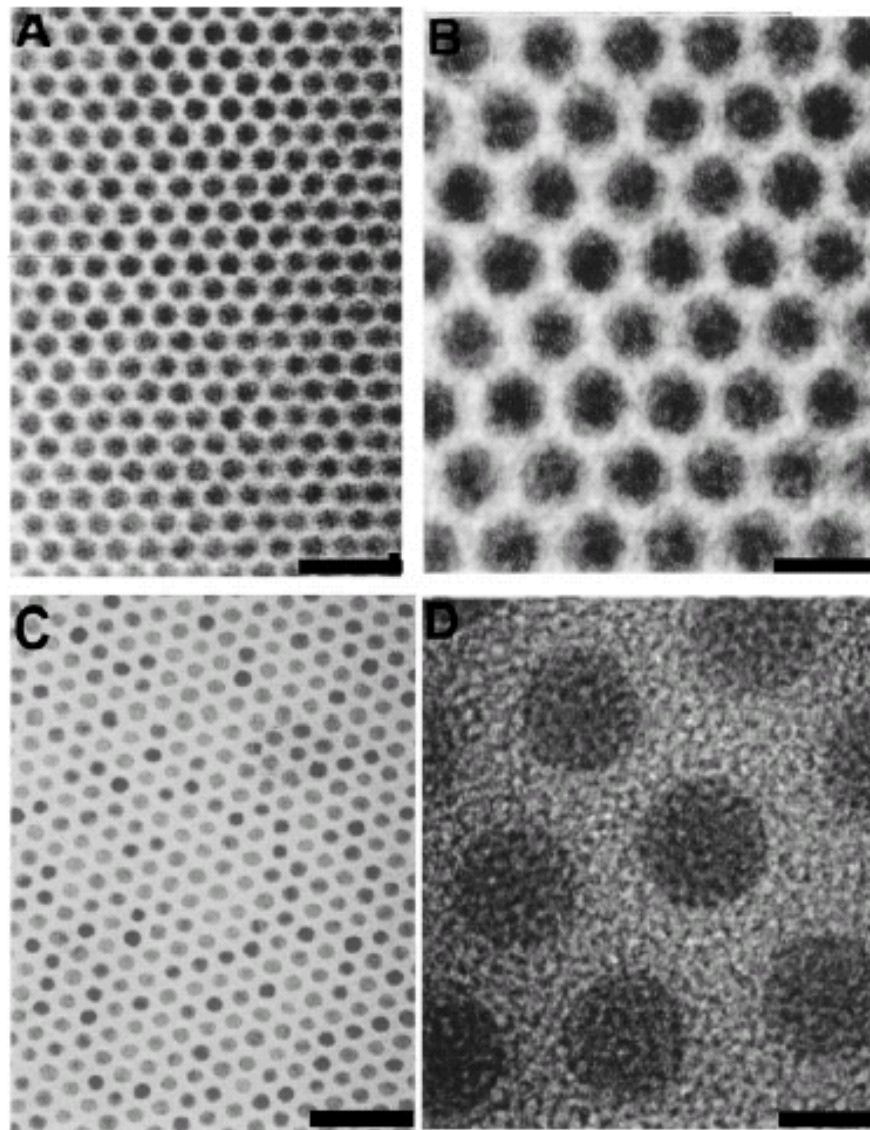
Figure 3 Large-field TEM images are employed to develop statistics on NC size and shape. A collection of 48 Å CdSe NCs at (*A*) low magnification (scale bar = 200 Å) and (*B*) higher magnification (scale bar = 80 Å) (45); monolayer of 80 Å Co NCs at (*C*) low magnification (scale bar = 500 Å) at (*D*) higher magnification (scale bar = 65 Å) (32).
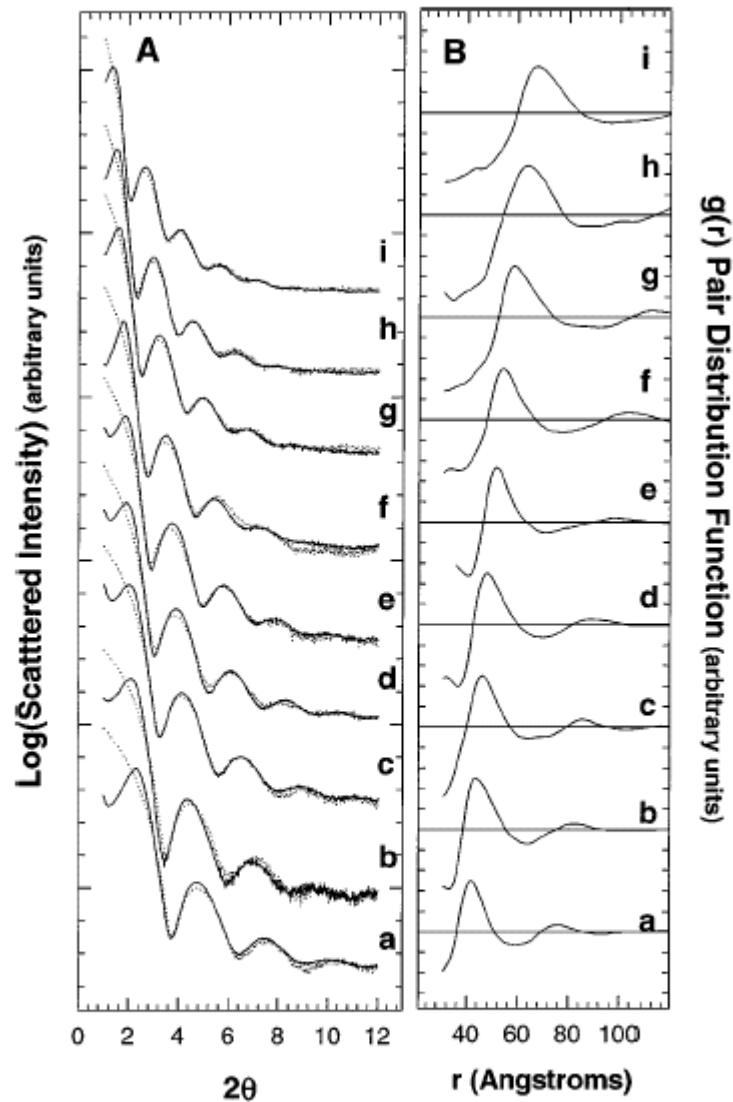
Figure 9 (*A*) Comparison of experimental SAXS patterns for CdSe NC samples, ranging from 32 to 72 Å in diameter, dispersed in PVB (dotted lines) and close-packed into glassy solids (solid line). (*B*) Pair distribution functions (PDFs), g(r) extracted from experimental SAXS data. TOPO/TOPSe caps maintain an average inter-particle spacing of 11 ± 1 Å.
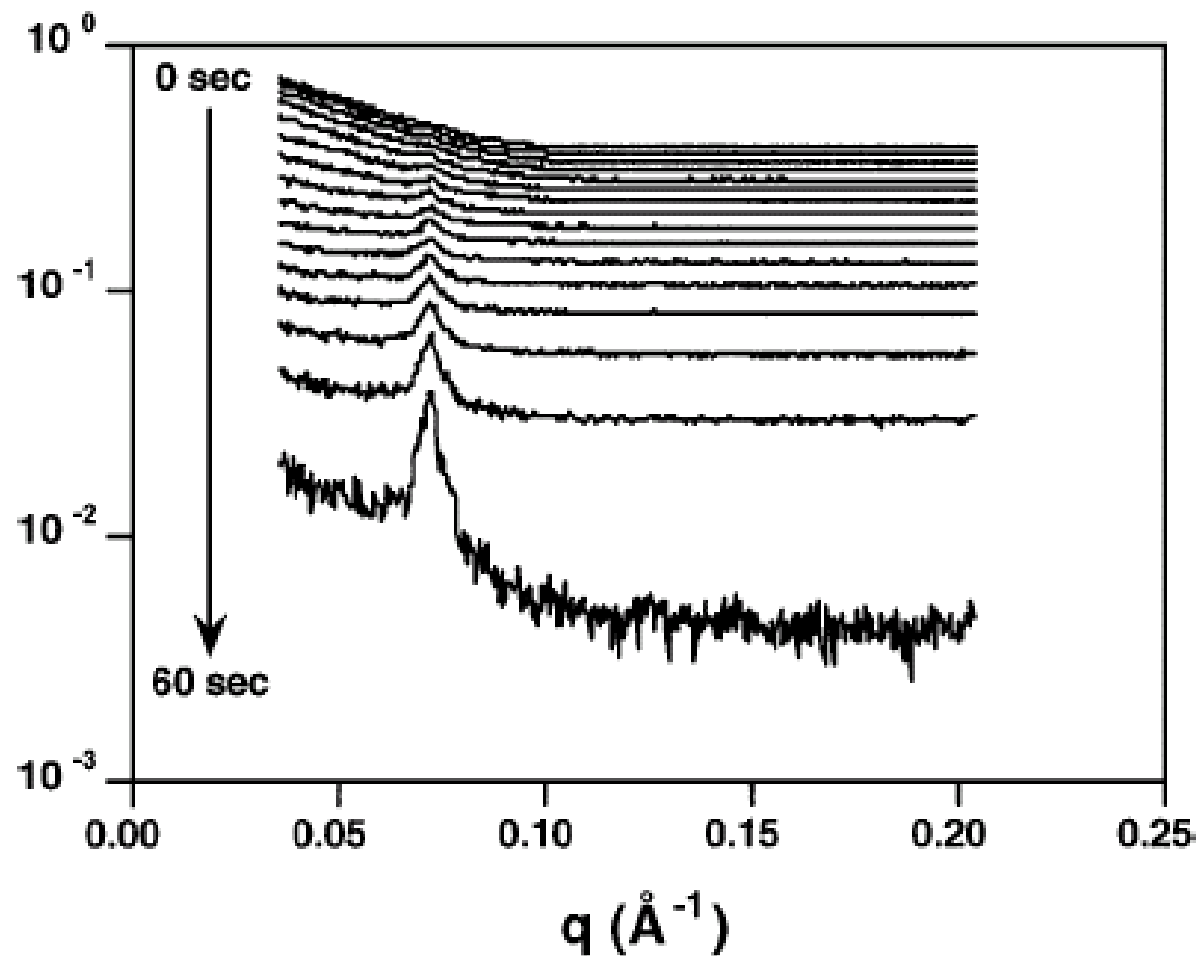
Figure 14 Time-resolved SAXS studies of a Ag superlattice as it self-assembles during evaporation from toluene. The sharp peaks that develop are from the inter-planar spacings of the deposited Ag superlattice (68).

Korgel BA, Fitzmaurice D. 1999. *Phys. Rev. B* 59:14191–20

Figure 15 Time-resolved SAXS studies of melting a Ag NC superlattice as a function of temperature. The disappearance of the sharp superlattice reflection upon heating indicates an order-to-disorder transition as the Ag NC superlattice is amorphized (69).
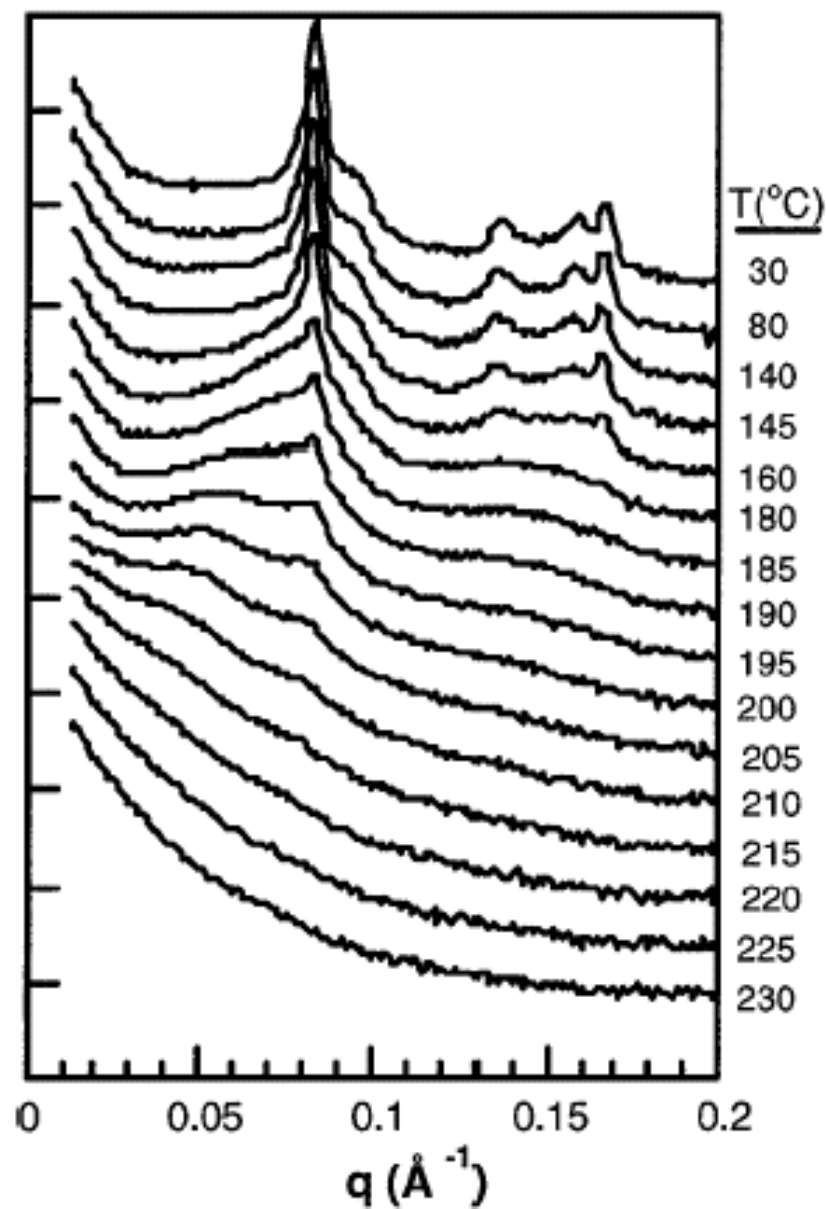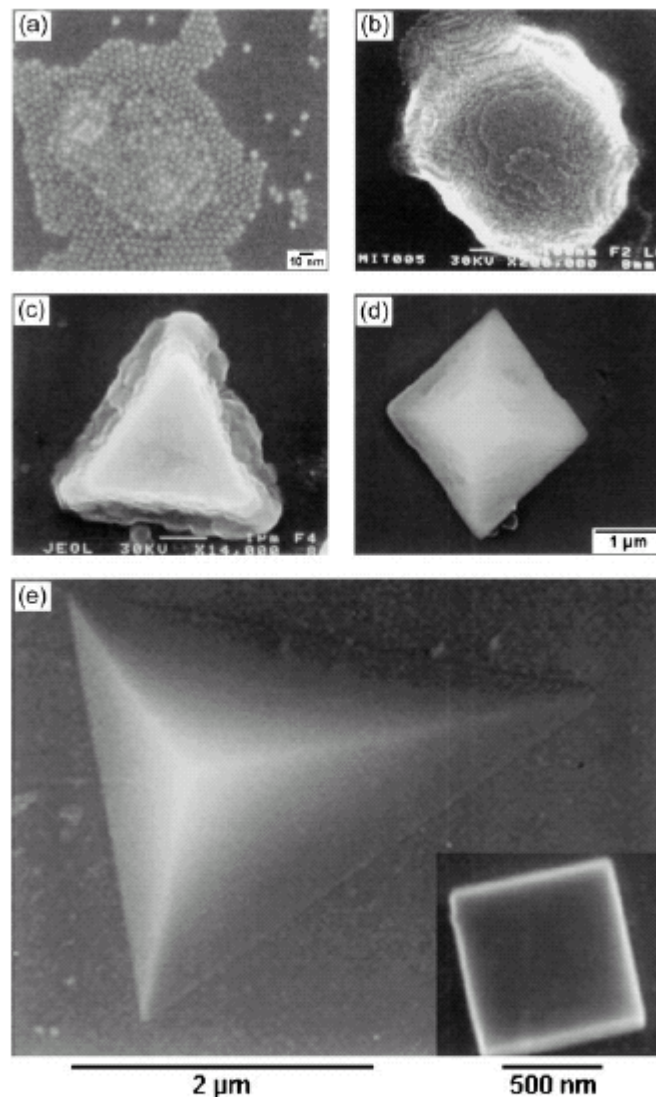
Figure 16 HRSEM images captures the morphology of self-assembled, close-packed islands and three-dimensional colloidal crystals of CdSe NCs. (*a*) The initial stages of growth for an island of ~750 62 Å CdSe NCs. (*b*) Three-dimensional growth forms more extensive islands of ordered 64 Å CdSe NCs. (*c*) One in a crop of similar size, incomplete $\langle 111 \rangle_{SL}$-oriented colloidal crystals of 57 Å CdSe NCs. (*d*) At <1% in a crop of colloidal crystals in the shape of a square pyramid may be found. (*e*) Slow growth rates form complete, regular colloidal crystals. Colloidal crystals of 48 Å NCs show the characteristic pyramidal shape of a $\langle 111 \rangle_{SL}$-oriented fcc structure. Ledges and terraces have closed off, forming vicinal $(100)_{SL}$ facets. The inset shows a $\langle 100 \rangle_{SL}$-oriented colloidal crystal from the same sample preparation (45).
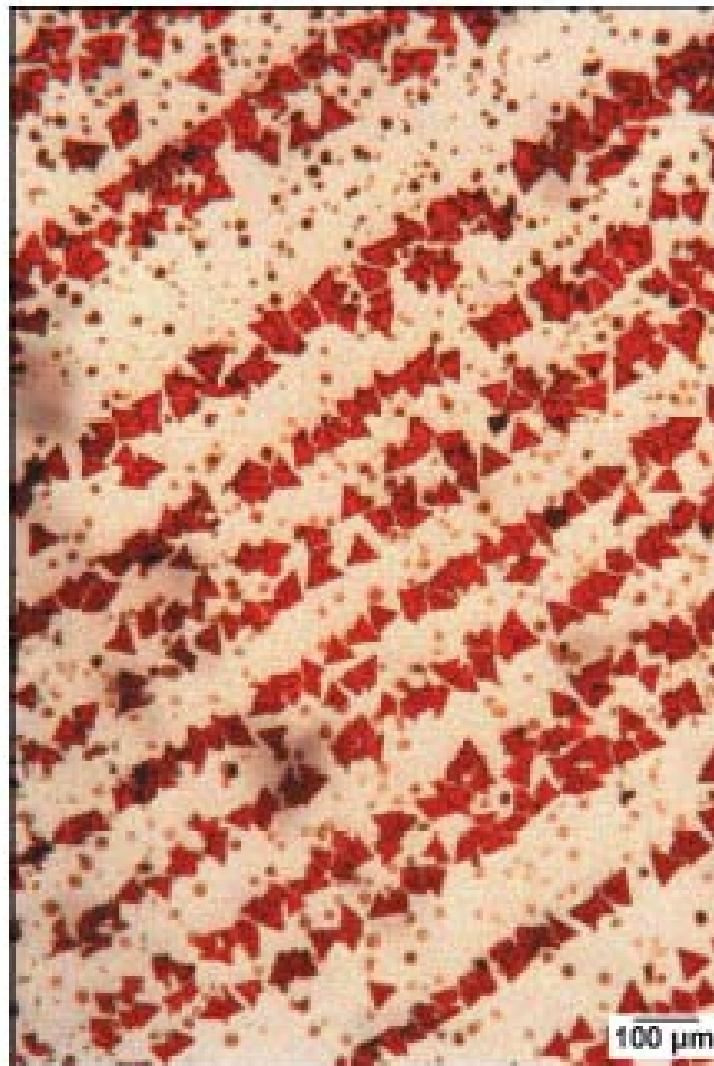
Figure 17 Optical micrograph of three-dimensional colloidal crystals of 57 Å CdSe QDs. The triangles form spokes that extend radially outward from the center on the bottom of a glass vial. The red color of the triangles is characteristic of the size-dependent absorption for the 57 Å CdSe NC building blocks (127).

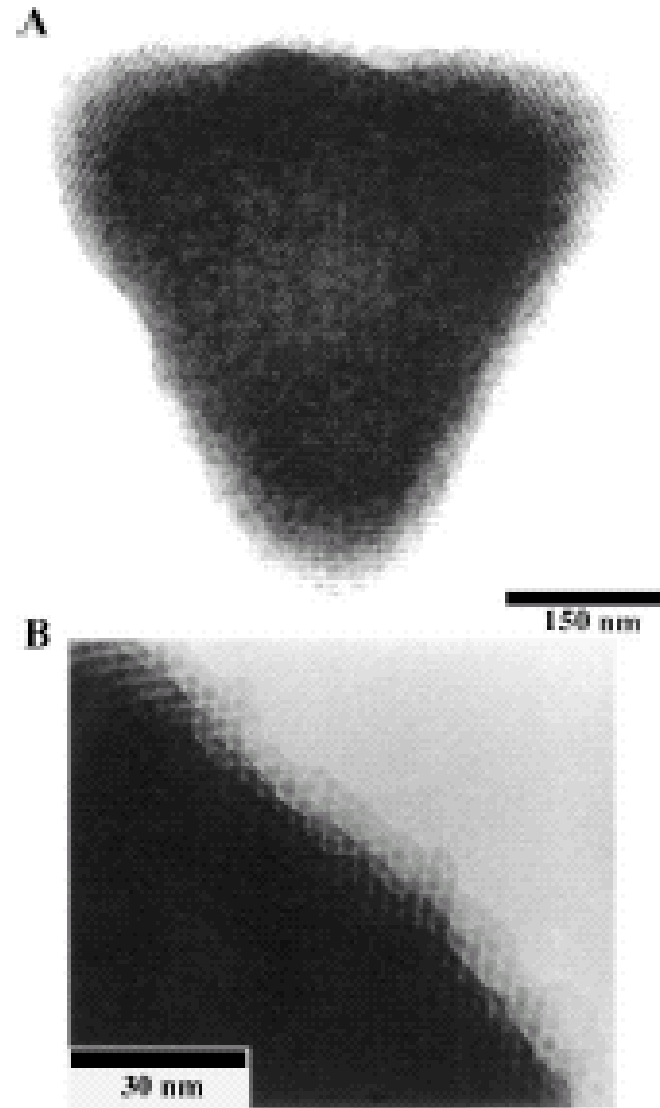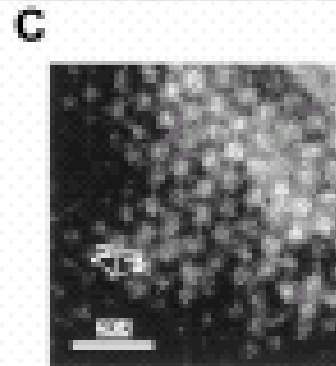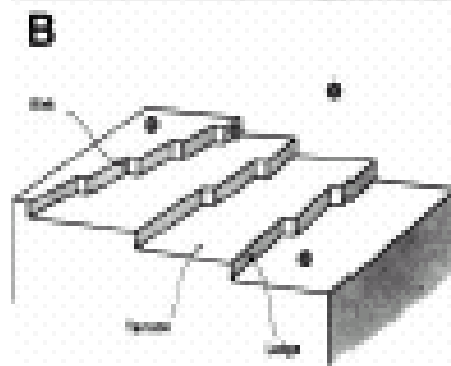**Figure 1** (*A*) TEM image of a faceted colloidal crystal prepared from 60 Å CdSe NCs. A star-shaped electron channeling pattern along the [111]SL dramatically demonstrates ordering in the single-domain colloidal crystal. (*B*) TEM image of one facet of the colloidal crystal showing the 60 Å CdSe NC building blocks.
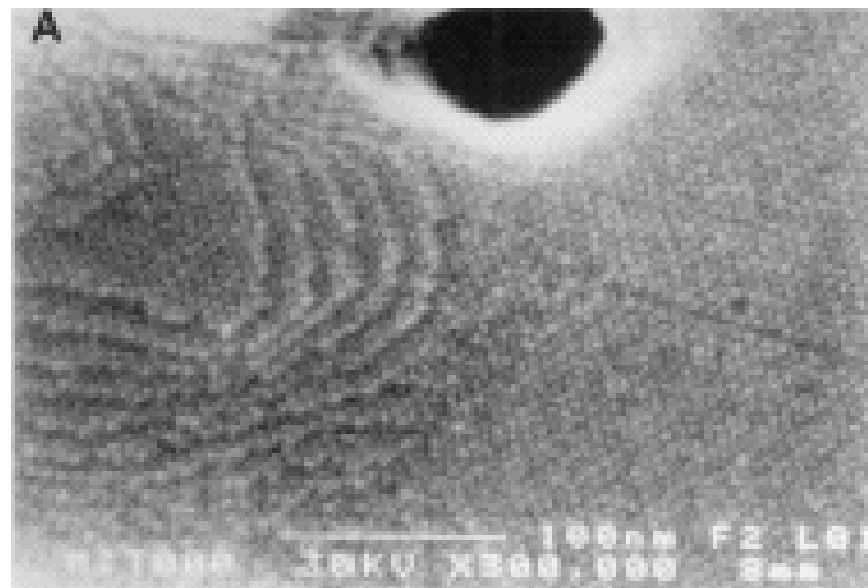
Figure 19 (A) HRSEM of a three-dimensional superlattice of 64 Å CdSe NCs grown epitaxially on an amorphous carbon substrate. Ordered rows of NCs form terraces, ledges, and kinks. (B) Superlattice growth is analogous to the terrace, ledge, kink model that describes monotonic crystal growth. (C) TEM image shows an ordered assembly of 64 Å InP NCs (120).
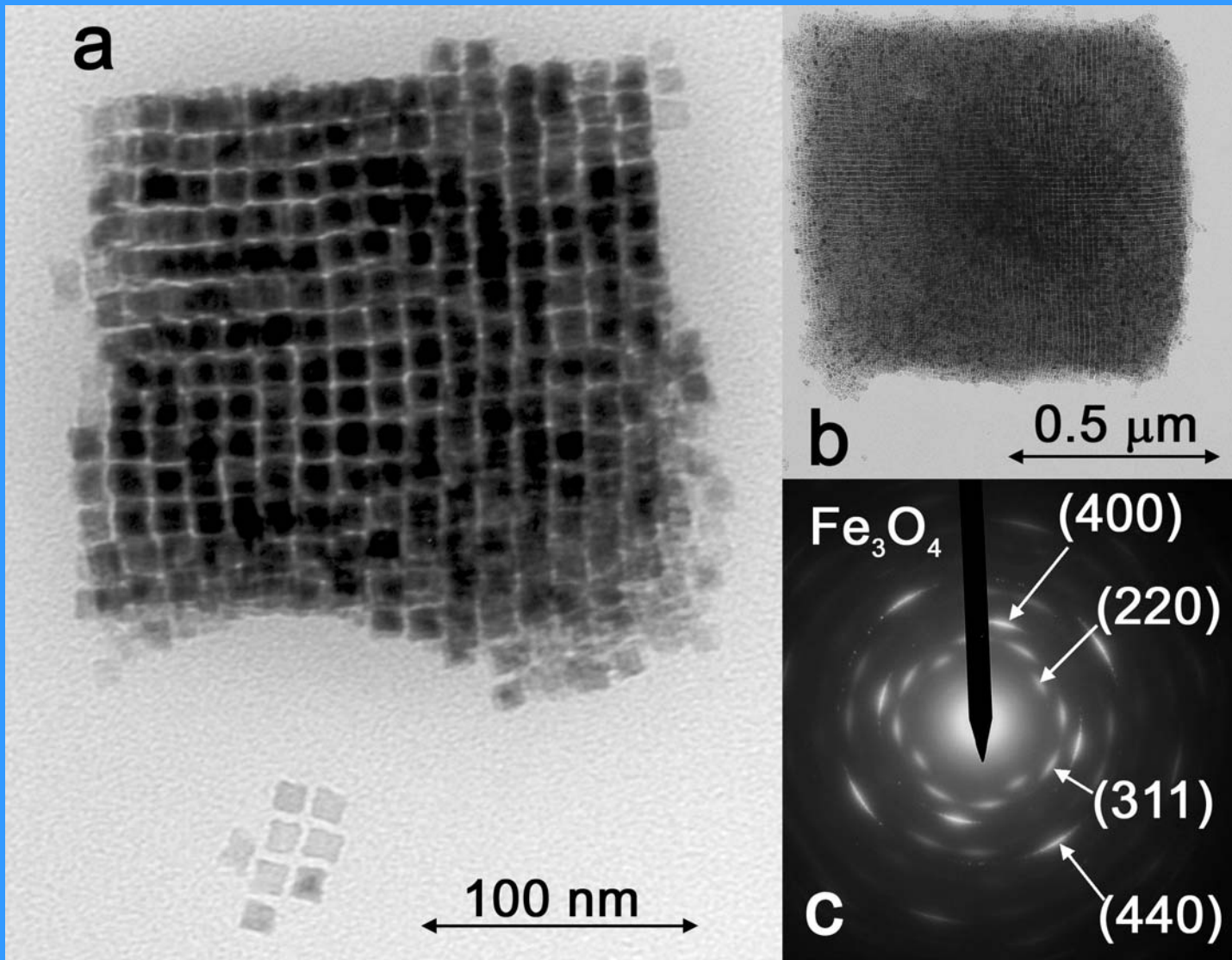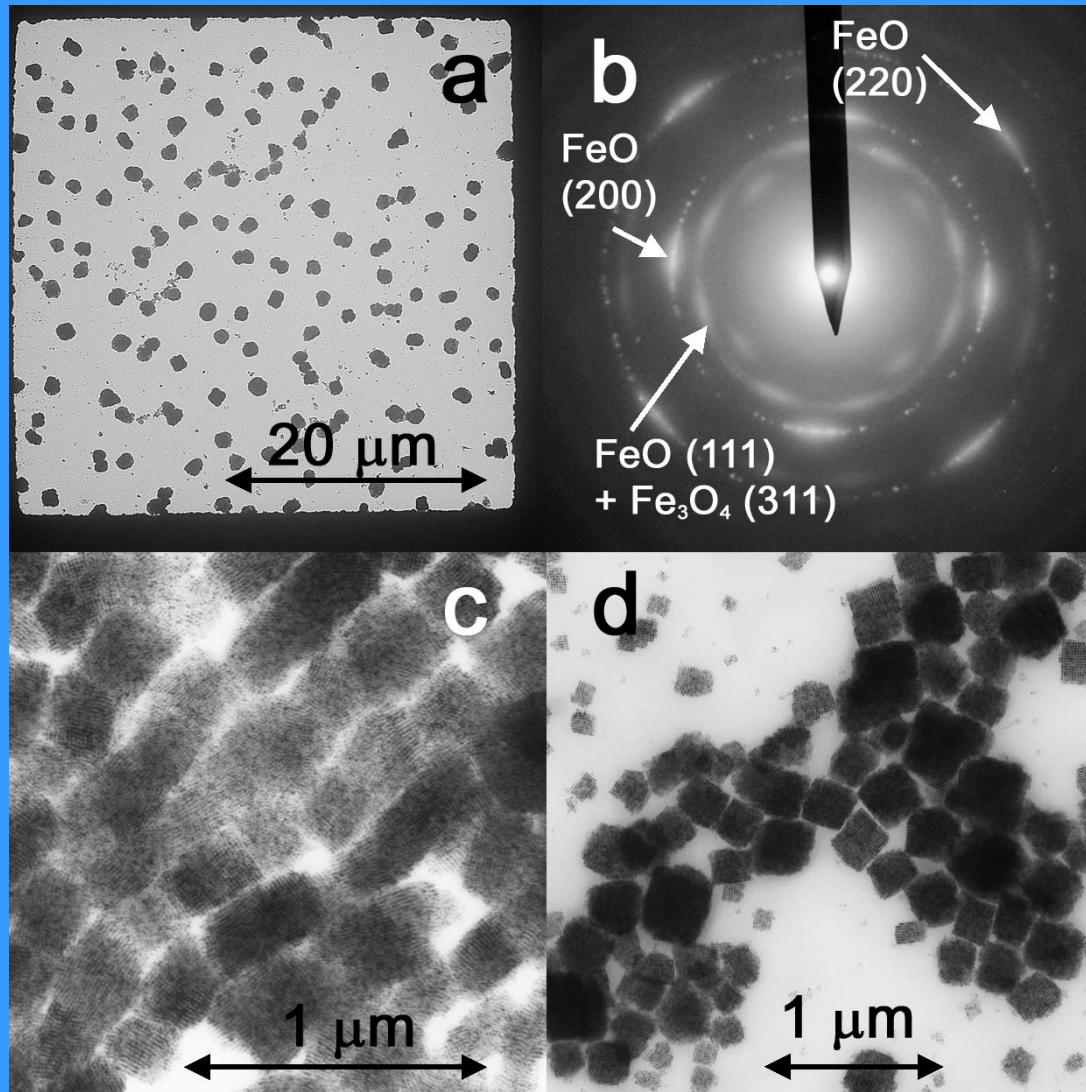
Figure 8: a) TEM image of a single cubic superlattice built of cubic FeO nanocrystals with 11 nm edge length. b) TEM image of a larger superlattice oxidized or decomposed after storage. c) SAED of the cubic superlattice in b) showing reflections for magnetite and orientational ordering in the superlattice.

Figure 4: a) LRTEM image of a quadratic subunit of a TEM grid showing nearly cubic superlattice built up of cubic wuestite nanocrystals. **b)** SAED of a selected superlattice with uneven but symmetric intensity distribution caused by preferred alignment of the particles (orientational ordering). **c)** TEM image of aligned superlattices arising during deposition of cubic FeO nanocrystals in a magnetic field parallel to the substrate. **d)** TEM image of aggregated superlattices deposited without external magnetic field.

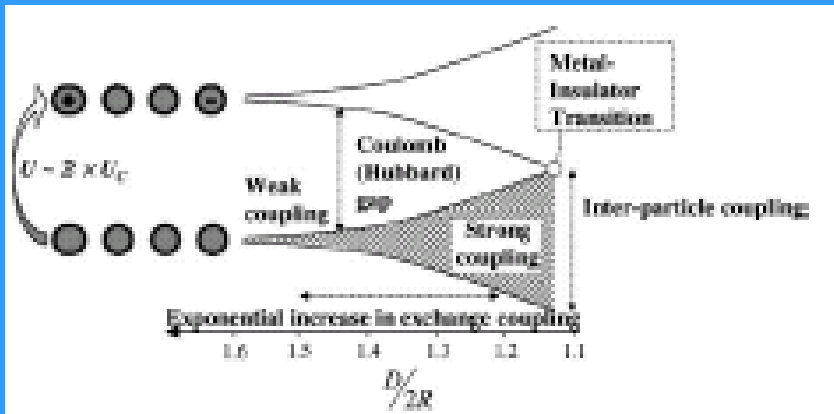# Fe$_3$O$_4$ nanoparticles

20 nm

Sun et al, *J. Am. Chem. Soc*. **2004**, *126*, 273.
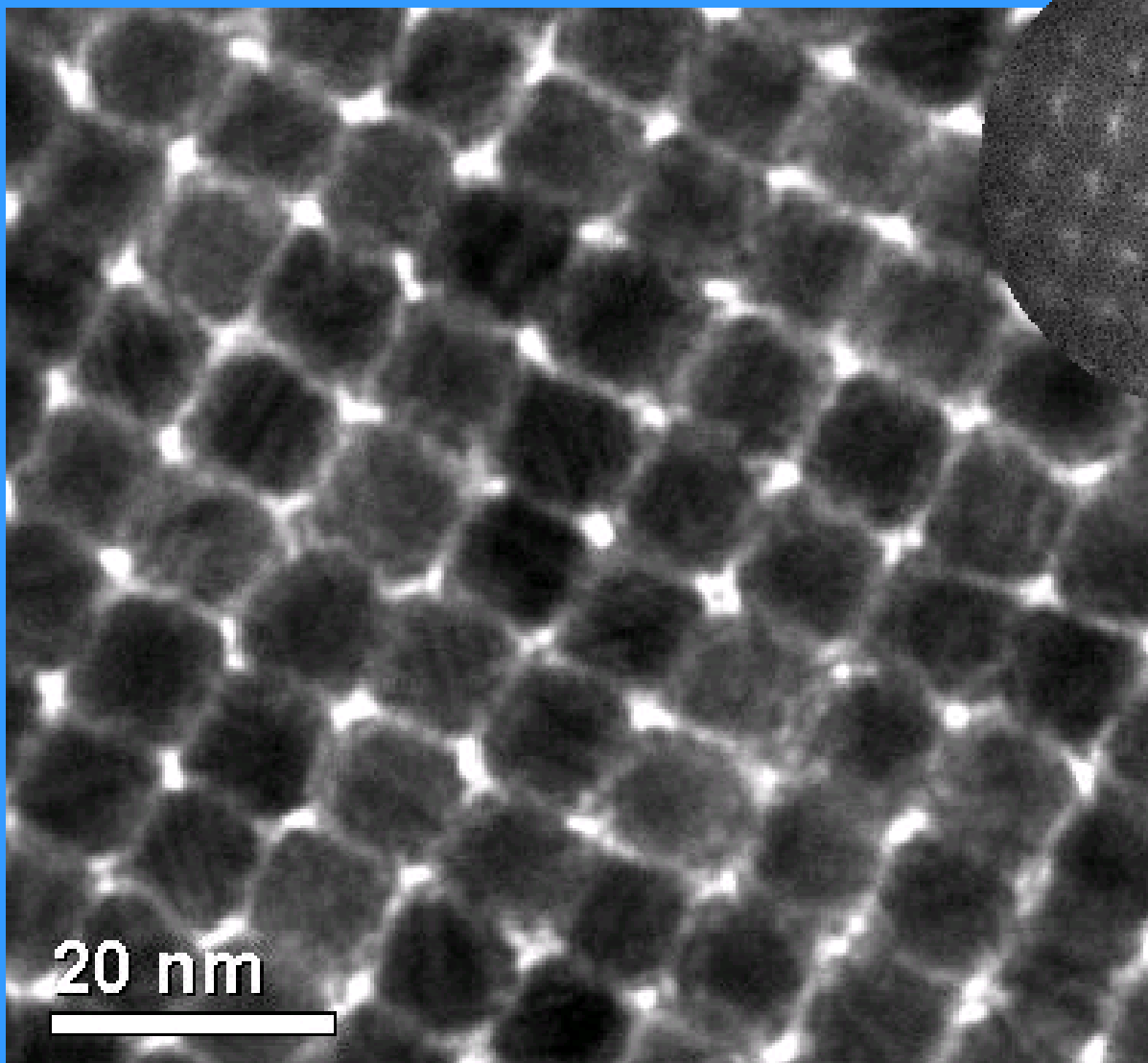
Shape induce crystal alignment
(14 nm MnFe$_2$O$_4$ nanoparticles)

(100) texture

(400)

(220) (311)

(511) (440)

2θ

(100) texture

H. Zeng, et al
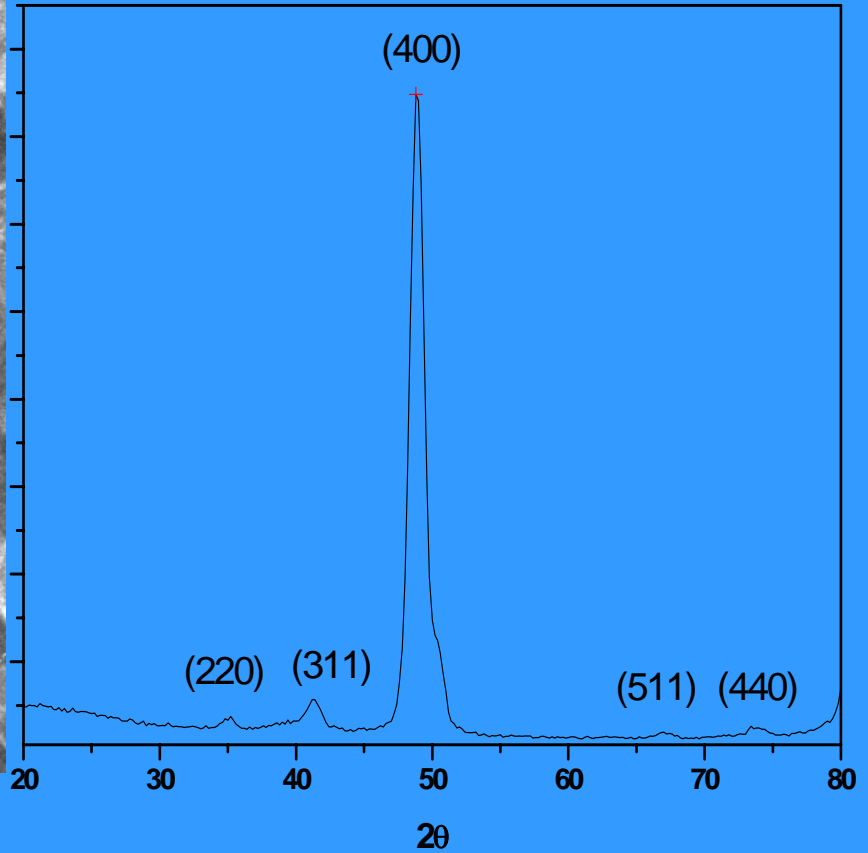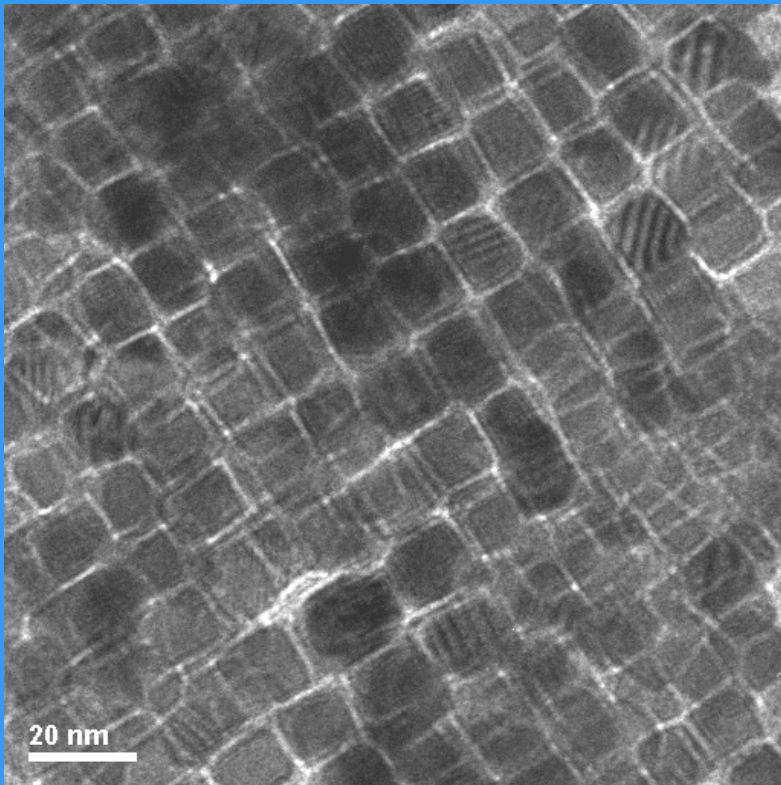
Figure 32 (Top) Cartoon of inter-particle interactions. At large inter-particle distances (D), NCs are electrically isolated and the superlattice is an insulator with a Coulomb bandgap. As the inter-particle distance decreases, exchange interactions become significant and the localized electronic wavefunctions of the individual NCs spread out over multiple NCs in the superlattice. In metal NC superlattices exchange interactions lead to an insulator-to-metal transition. (Bottom) (a) dI/dV or normalized density of states (NDOS) versus applied V for (a) decanethiol-capped Ag NCs maintaining D ~ 1.2 nm and (b) hexanethiol-capped Ag NCs providing D ~ 0.5 nm (195).
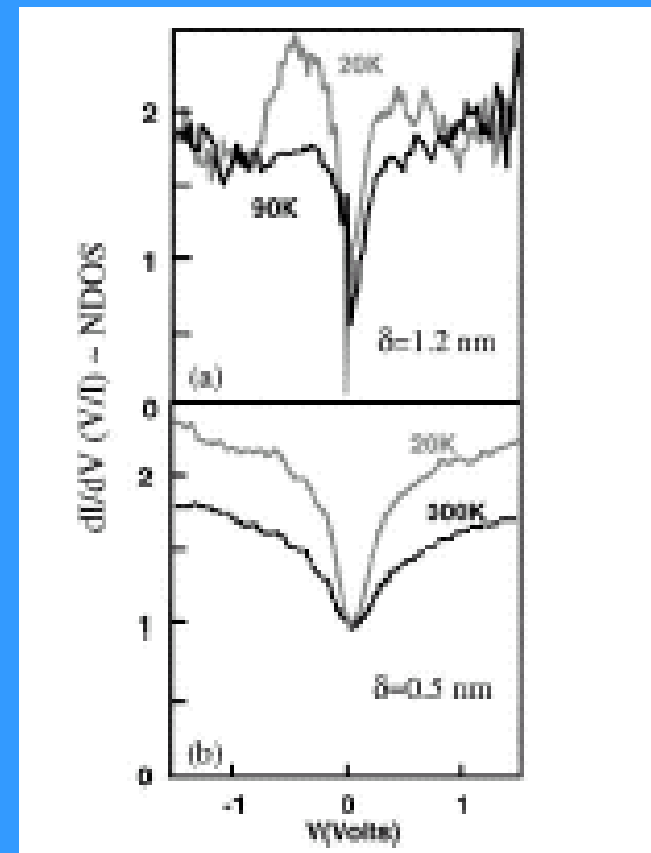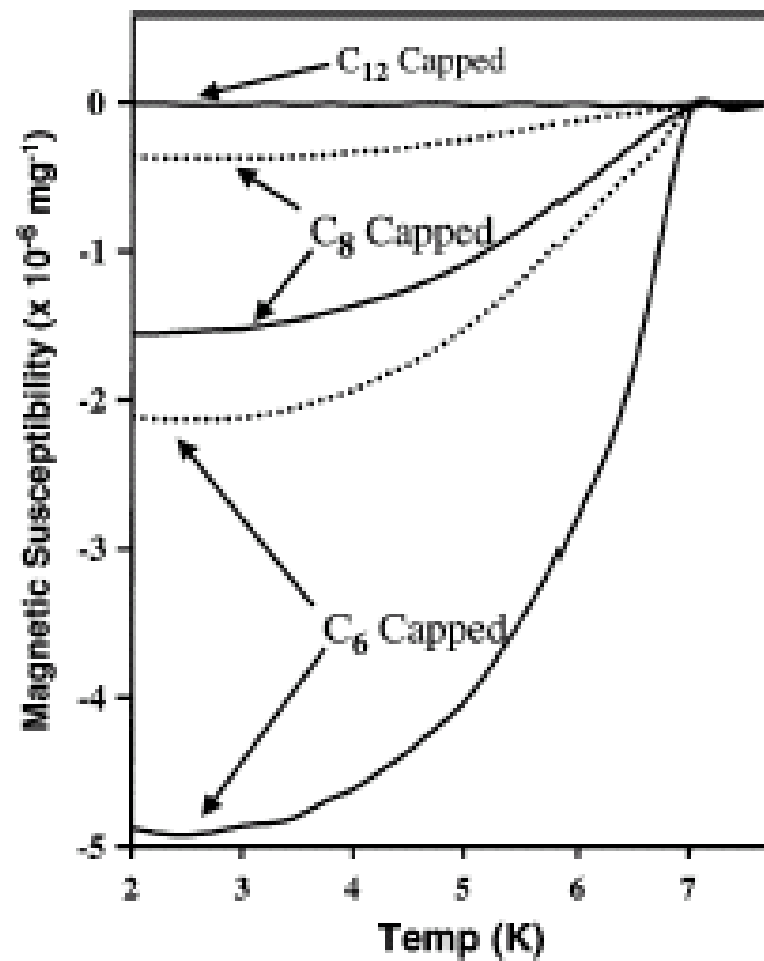
Figure 33 Magnetic susceptibility versus temperature at 400 Gauss for Pb QD assemblies separated by dodecane- (C_{12}), octane- (C_8), and hexane- (C_6)carboxylates (1%).